Electronic Structures of Zinc and Palladium Tetraazaporphyrin Derivatives Controlled by Fused Benzo Rings

Hideya Miwa, Kazuyuki Ishii, and Nagao Kobayashi*[a]

Abstract: Zinc and palladium tetracyclic aromatic complexes lying structurally between tetraazaporphyrin (TAP) and phthalocyanine (Pc), that is, monobenzo-, adjacently dibenzo-, oppositely dibenzo-, and tribenzo-fused TAPs, have been prepared, and their electronic structures investigated by electronic absorption, magnetic circular dichroism (MCD), fluorescence, phosphorescence, and time-resolved electron paramagnetic resonance (TREPR) spectroscopy, as well as cyclic voltammetry. The last-named indicated that the first oxidation potentials shift to more negative values with increasing number of the fused benzo rings, but also suggested that the first reduction potential apparently has no correlation with the size and symmetry of the π-conjugated systems. However, this latter behavior is reasonably interpreted by the finding that the effect of the fused benzo rings on destabilization of the LUMO depends on the orbital to which they are fused (i.e., whether it is an e_{gx} or e_{gy} orbital), since the LUMOs of TAP complexes are degenerate with D_{4h} symmetry. The energy splitting of the LUMOs, that is, ΔLUMO, was evaluated experimentally for the first time by analyzing the relationship between the first reduction potential and the size and shape of the π-conjugated system. Electronic absorption and MCD measurements indicate that the lowest excited singlet states are split in the case of the low-symmetry TAP derivatives, although these excited states are degenerate for Pc and TAP with D_{4h} symmetry. These energy splittings ΔE_{SS} correlate well with the ΔLUMO values. To investigate the electronic structures in the lowest excited triplet state, zero-field splitting (zfs) was analyzed by time-resolved EPR (TREPR) spectroscopy. The energy splitting in the lowest excited triplet state, ΔE_{TT} was quantitatively evaluated from the temperature dependence of the zfs or spin–orbit coupling of the Pd complexes. Consequently, it is demonstrated that ΔLUMO, ΔE_{SS}, and ΔE_{TT} values exhibiting a mutually good relationship can be determined experimentally.

Keywords: cyclic voltammetry · electronic structure · EPR spectroscopy · luminescence · macrocyclic ligands

Introduction

Phthalocyanines (Pcs) are important compounds not only in practical areas such as dyes, pigments, catalysts for controlling sulfur emissions, photoconducting agents in photocopiers, photovoltaic cell elements for energy generation, optical disks, and deodorants, but also in terms of nonlinear optics, photodynamic cancer therapy, liquid crystals, chemical sensors, molecular electronics, Langmuir–Blodgett films, conducting polymers, and electrochromic display devices.[1–3] Furthermore, Pcs and tetraazaporphyrins (TAPs) are analogous to porphyrins, which play important roles in biological systems such as photosynthetic reaction centers, heme, and vitamin B_{12}.[4–6] The chemistry of Pcs and TAPs was thus one of the most significant fields of science in the 20th century, and further development is still required into the 21st century.

In addition to easy synthesis and high stability, the effectiveness of Pcs and TAPs originates from their redox activity and intense π–π* transitions in the visible region,[1–3] which depend mainly on the four frontier orbitals, the HOMO, nearby HOMO−1, and degenerate LUMOs (in D_{4h} symmetry, these are a_{1u}, a_{2u}, and e_g orbitals, respectively). To realize novel properties, control of the π-conjugated system by fusion of aromatic rings onto the pyrrole rings of the TAP skeleton has been attempted systematically to produce several Pcs, TAPs, naphthalocyanines, anthoracyanines,[7,8] and low-symmetry derivatives thereof.[9–13] However, the essential properties of the frontier orbitals and lowest excited singlet (S_1) and triplet (T_1) states have not been clarified for low-symmetry Pc and TAP derivatives, though some elec-

[a] Dr. H. Miwa, Dr. K. Ishii, Prof. Dr. Dr. N. Kobayashi
Department of Chemistry
Graduate School of Science
Tohoku University
Sendai 980–8578 (Japan)
Fax: (81) 22-217-7719
E-mail: nagaok@mail.tains.tohoku.ac.jp

Supporting information for this article is available on the WWW under http://www.chemeurj.org/ or from the author.

DOI: 10.1002/chem.200400328

tronic absorption, magnetic circular dichroism (MCD), and cyclic voltammetry (CV) studies have been reported, together with molecular orbital (MO) calculations.[7–13]

In this work, we synthesized zinc and palladium complexes of TAP, Pc, and their low-symmmetry derivatives systematically (Scheme 1), and investigated the relationships between the frontier orbitals, S_1, T_1, and the π-conjugated systems using electronic absorption, MCD, CV, luminescence, and time-resolved electron paramagnetic resonance (TREPR) measurements together with MO calculations. In the case of TAP and Pc complexes with D_{4h} symmetry, the S_1 (S_{1x} and S_{1y}) and T_1 (T_{1x} and T_{1y}) states are degenerate because of the degeneracy of the LUMOs (e_{gx} and e_{gy}).[14] Since fused benzo rings result in a breaking of the symmetry (**1M**, **2AdM**, and **3M**$\rightarrow C_{2v}$; **2OpM**$\rightarrow D_{2h}$; M = Zn or Pd; Scheme 1), the energy splittings between the S_{1x} and S_{1y} states (ΔE_{SS}), between the T_{1x} and T_{1y} states (ΔE_{TT}), and between the LUMOs (ΔLUMO) are among the most important electronic properties for characterizing low-symmetry Pc derivatives. Here novel methods for evaluating the ΔE_{TT} and ΔLUMO values are shown, in addition to analysis of ΔE_{SS}. Important features are: 1) The first oxidation and reduction potentials were evaluated by CV measurements. From the CV results and MO calculations, we not only clarified the relationship between the MO energy and the π-conjugated system, but also elaborated a novel method for experimentally determining the ΔLUMO values. 2) The S_1 properties were investigated by electronic absorption, MCD, and fluorescence spectra. The ΔE_{SS} values were quantitatively determined by simultaneous band-deconvolution analyses of electronic absorption and MCD spectra, which are reproduced well by configuration interaction (CI) calculations. 3) The T_1 properties were investigated by phosphorescence and TREPR measurements. By analyzing the temperature dependence of zero-field splitting (zfs) or spin–orbit coupling (SOC) of the Pd complexes, the ΔE_{TT} values were experimentally determined. The ΔLUMO, ΔE_{SS}, and ΔE_{TT} values obtained are compared, and the relationship between these energies and the π-conjugated system is clarified.

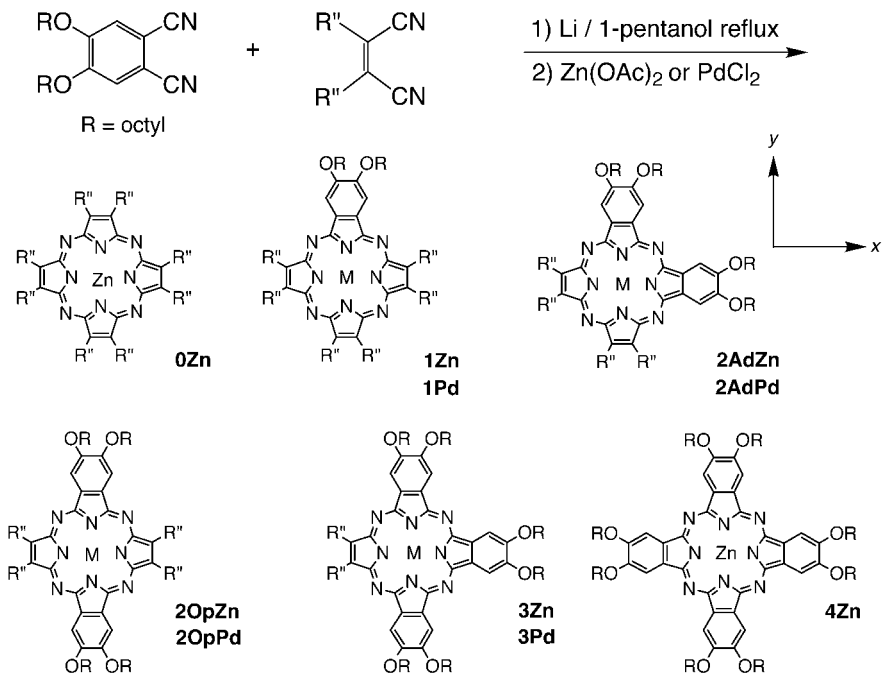

Scheme 1. Synthesis and molecular structures of low-symmetry TAP derivatives, together with their abbreviations. For Zn and Pd complexes, R″ denotes phenyl and *p-tert*-butylphenyl groups, respectively.

Results

Electrochemistry: To obtain information on the HOMO and LUMO energies, CV measurements were carried out for the zinc complexes (Figure 1), and the electrochemical data are summarized in Table 1. Since the central zinc ion is redox-inactive, the observed two reduction couples and one oxidation couple originate from the ligand.[15,16] The first oxidation potential, reflecting the HOMO energy, decreases in the order **0Zn** (0.65 V) > **1Zn** (0.50 V) > **2AdZn** (0.36 V) ≈ **2OpZn** (0.34 V) > **3Zn** (0.19 V) > **4Zn** (0.08 V). The almost identical first oxidation potentials of **2OpZn** and isomeric **2AdZn** indicate that the HOMO energy correlates well with the size of the π-conjugated system. However, the first reduction potential, corresponding to the LUMO energy,

Table 1. Electrochemical data [V versus Fc^+/Fc] of the zinc complexes (DC = diffusion coefficient).[a]

Compd	$E^{1+/0}$	$E^{0/1-}$	$E^{1-/2-}$	ΔE_{o-r}[b]	DC [10^{-6} cm^2 s^{-1}]
0Zn	0.65[c]	−1.28 (0.09)	−1.60 (0.08)	1.93	1.31[d]
1Zn	0.50 (0.09)	−1.29 (0.08)	−1.59 (0.07)	1.79	1.52[d]
2AdZn	0.36 (0.08)	−1.46 (0.07)	−1.73[c]	1.82	1.40[e]
2OpZn	0.34 (0.08)	−1.29 (0.08)	−1.59 (0.08)	1.63	1.44[f]
3Zn	0.19 (0.10)	−1.47 (0.08)	−1.84 (0.08)	1.66	1.33[f]
4Zn	0.08[c]	−1.65 (0.08)	−2.03 (0.09)	1.73	0.94[d]

[a] Potential differences between cathodic and anodic peaks at a sweep rate 50 mV s^{-1} are shown in parentheses. [b] Difference between the first oxidation and reduction potentials. [c] These potentials were determined from differential pulse voltammograms, since the cyclic voltammograms are not clear. [d] From the current peaks at the first reduction wave. [e] From the current peaks at the first oxidation wave. [f] From the current peaks at the first reduction and oxidation waves.

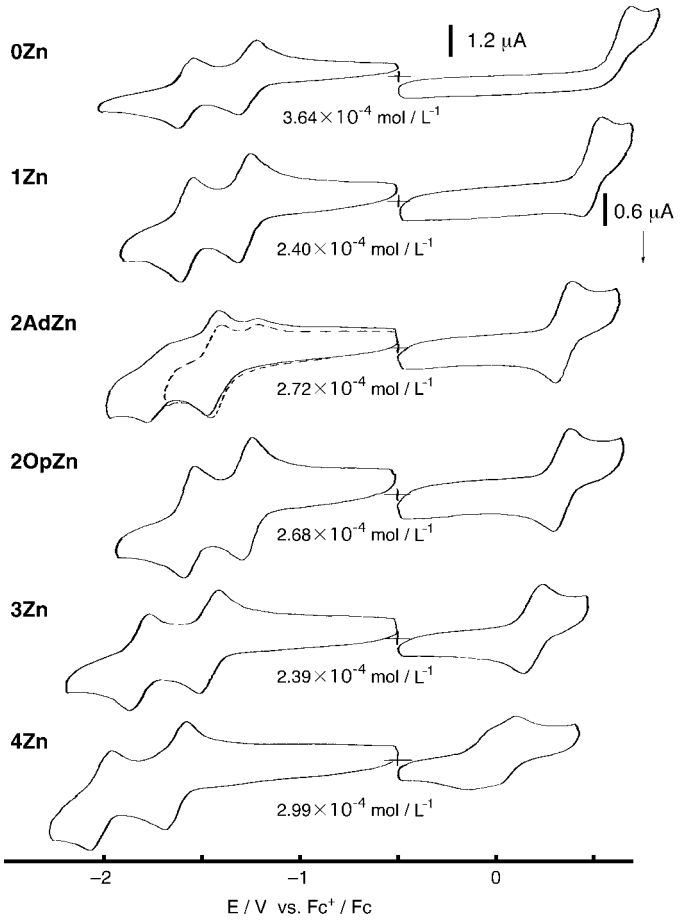

Figure 1. Cyclic voltammograms of the zinc complexes obtained at a scan rate of 50 mV s^{-1} in *o*-DCB solution containing 2.5×10^{-2} M pyridine and 0.1 M TBAP.

shifts to negative values in a different order: **0Zn** (−1.28 V) ≈ **1Zn** (−1.29 V) ≈ **2OpZn** (−1.29 V) > **2AdZn** (−1.46 V) ≈ **3Zn** (−1.47 V) > **4Zn** (−1.65 V). Thus, at first glance, the LUMO energy appears to have no relationship to the number of fused benzo rings, in contrast to the HOMO energy. The difference between the first oxidation and reduction potentials ΔE_{o-r} decreases in the order **0Zn** (1.93 V) > **2AdZn** (1.82 V) > **1Zn** (1.79 V) > **4Zn** (1.73 V) > **3Zn** (1.66 V) > **2OpZn** (1.63 V).

Electronic absorption and MCD spectra: Electronic absorption and MCD spectra of the zinc complexes are shown in Figure 2,[17] and the data summarized in Table 2. In the electronic absorption spectra, intense $Q_{0\text{-}0}$ bands are seen for **0Zn** (637 nm) and **4Zn** (677 nm), respectively. In the MCD spectra, the observed dispersion-type Faraday *A* terms correspond to the $Q_{0\text{-}0}$ bands, that is, the S_1 states are degenerate for **0Zn** and **4Zn**. On the other hand, the Q bands are split into intense Q_y (the $S_0\rightarrow S_{1y}$ (E_{uy}) transition) and Q_x (the $S_0\rightarrow S_{1x}$ (E_{ux}) transition) bands for the low-symmetry TAP derivatives **1Zn** (C_{2v}; 625 and 667 nm) and **2OpZn** (D_{2h}; 605 and 708 nm). For **3Zn**, three intense bands appear at 628, 642, and 690 nm in the Q-band region. Since relatively intense vibronic bands with vibrational energies of 1300–1600 cm^{-1} are seen for all the zinc complexes, these bands at 642 and 690 nm are attributed to the $Q_{y0\text{-}0}$ and $Q_{x0\text{-}0}$ bands, respectively, and the band at 628 nm is assigned as a vibronic band. This assignment results in plausible vibrational energies in the Q_y (1580 cm^{-1}) and Q_x (1430 cm^{-1}) bands. In addition, this assignment of Q_x and Q_y bands is unambiguously supported by the Faraday *B* terms of opposite sign in the MCD spectra, which are consistent with the molecular structure having only C_2 axes. In the case of **2AdZn**, Q-band splitting is not evident in the electronic absorption spectrum (654 nm), and a dispersion-type MCD signal is observed corresponding to the $Q_{0\text{-}0}$ absorption band. This single Q band is characteristic of adjacently substituted derivatives.[9–13] For other low-symmetry TAP derivatives, the signs of the MCD *B*-term envelopes are minus and plus for the Q_x and Q_y bands, respectively, that is, the energy splitting between the HOMO and HOMO−1 is larger than that between the LUMO and LUMO+1.[18]

To determine the energy levels quantitatively, band-deconvolution analyses were carried out.[19,20] The calculated $Q_{x0\text{-}0}$ and $Q_{y0\text{-}0}$ bands are shown in Figure 2 (broken lines). Consequently, the energy splitting of the Q band ΔE_{SS} decreases in the order **2OpZn** (2380 cm^{-1}) > **3Zn** (1040 cm^{-1}) > **1Zn** (960 cm^{-1}) > **2AdZn** (280 cm^{-1}). The Q_x band shifts to the lower energy side in the order **0Zn** (1.57×10^4 cm^{-1}) > **2AdZn** (1.52×10^4 cm^{-1}) > **1Zn** (1.50×10^4 cm^{-1}) > **4Zn** (1.48×10^4 cm^{-1}) > **3Zn** (1.45×10^4 cm^{-1}) > **2OpZn** (1.41×10^4 cm^{-1}). This order is the same as that of the ΔE_{o-r} value reflecting the size of the HOMO–LUMO energy gap. In the Soret-band region, because of the broad bandwidth and low reso-

Table 2. Electronic absorption and MCD spectral data.

Compd	Abs. λ [nm] ($10^{-4}\varepsilon$ [dm^{3}mol^{-1}cm^{-1}])	MCD λ [nm] (10^{-5} [θ]$_M$ [deg dm^{3}mol^{-1}cm^{-1}T^{-1}])
0Zn	383 (9.97), 585 (2.46), 637 (14.1)	362 (0.806), 388 (−1.69), 581 (2.92), 629 (11.5), 644 (−16.9)
1Zn	377 (7.37), 577 (1.51), 625 (6.89), 667 (7.73)	361 (0.721), 386 (−1.23), 608 (3.83), 665 (−5.08)
2AdZn	376 (10.2), 592 (3.12), 654 (16.7)	354 (0.941), 382 (−1.89), 593 (4.16), 645 (16.6), 659 (−22.9)
2OpZn	359 (5.90), 389 (5.95), 605 (6.60), 645 (1.49), 708 (10.0)	321 (−0.140), 353 (0.642), 388 (−0.801), 605 (4.25), 641 (−1.20), 709 (2.69)
3Zn	364 (7.68), 583 (1.98), 628 (6.51), 642 (6.66), 690 (11.6)	311 (−0.237), 353 (0.886), 380 (−1.21), 583 (1.71), 623 (6.34), 643 (1.82), 660 (−1.49), 689 (−6.38)
4Zn	295 (4.69), 364 (10.4), 611 (4.25), 648 (4.06), 677 (28.6)	348 (1.13), 370 (−2.18), 613 (7.55), 643 (4.36), 672 (50.2), 682 (−57.4)
1Pd	343 (5.97), 450 (1.98), 562 (2.31), 613 (6.90), 655 (7.21)	361 (−0.633), 418 (0.250), 467 (−0.220), 562 (1.67), 597 (3.20), 654 (−4.01)
2AdPd	305 (5.88), 338 (6.21), 440 (2.24), 581 (3.60), 640 (15.1)	356 (−0.675), 410 (0.210), 455 (−0.288), 580 (3.58), 610 (2.06), 632 (9.92), 645 (−16.8)
2OpPd	310 (5.68), 453 (1.55), 547 (1.90), 593 (5.62), 632 (1.75), 692 (9.08)	310 (0.093), 352 (−0.409), 400 (0.155), 457 (−0.159), 549 (0.838), 593 (3.22), 628 (−1.08), 691 (−2.14)
3Pd	300 (7.80), 408 (2.17), 573 (3.06), 617 (6.86), 629 (7.22), 674 (9.86)	307 (1.91), 340 (−5.83), 394 (0.149), 448 (−0.241), 574 (2.35), 610 (4.37), 646 (−1.88), 673 (−4.80)

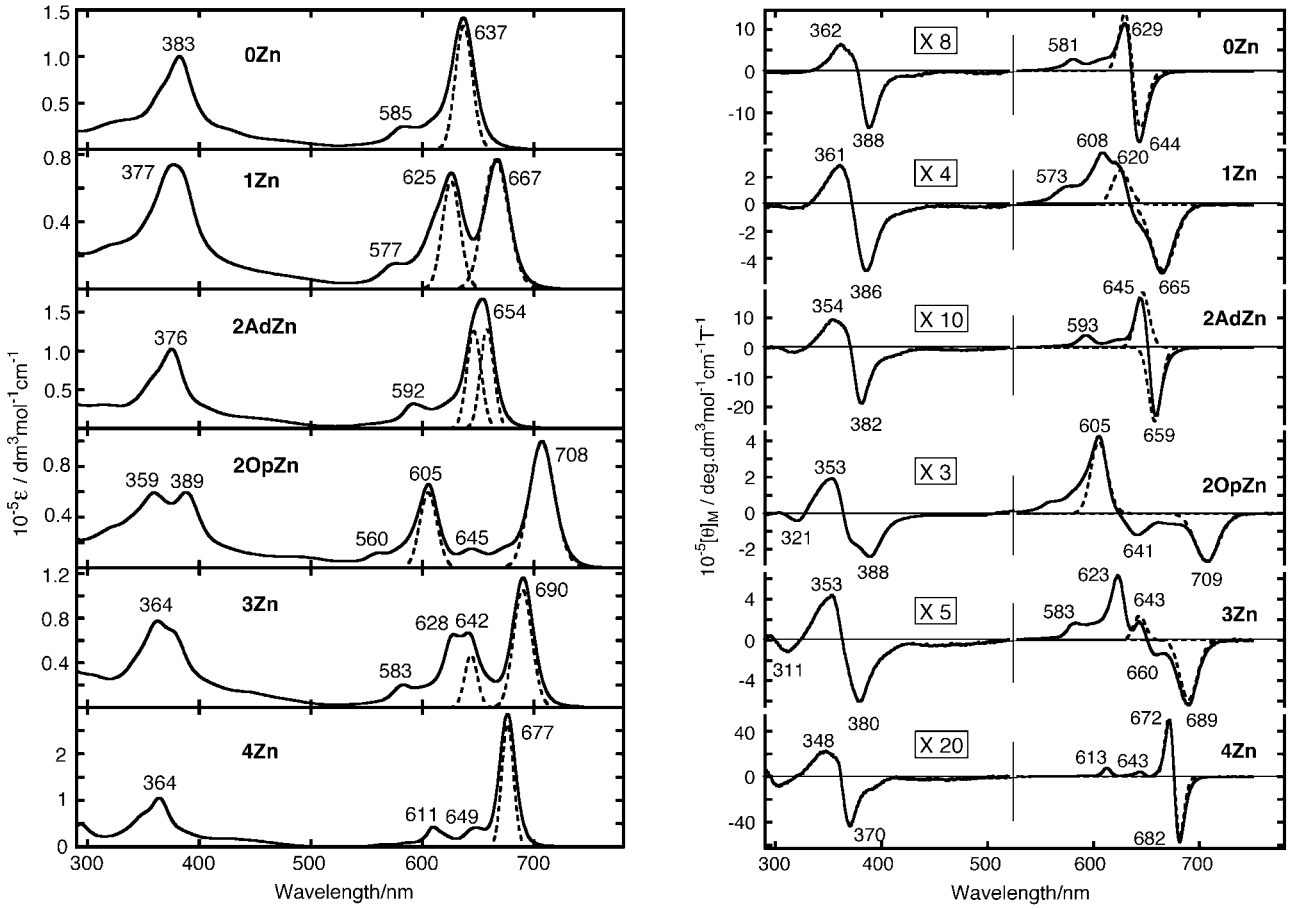

Figure 2. Electronic absorption (left) and MCD (right) spectra of the zinc complexes in toluene containing 1×10^{-2} M pyridine. The Q_x and Q_y bands evaluated by band-deconvolution analyses are also shown (broken lines).

lution, a clear band splitting is seen only for **2OpZn** (359 and 389 nm). Thus, the Soret-band splitting is the largest for **2OpZn**, similar to the Q band.

Electronic absorption and MCD spectra of the palladium complexes are shown in Figure 3. While the Q-band splitting of the Pd complexes is similar to that of the corresponding Zn complexes, the Q band shifts to the higher energy side relative to the zinc complexes by 300–400 cm^{-1}. This blue shift of the Q band can be interpreted as due to destabilization of the LUMO by interaction between the LUMO of the ligand and the d_π orbital of the Pd atom.[14] This idea is in accord with the small *B*/*D* values obtained for the Pd complexes, which have been shown to originate from the interaction between the LUMO and the d_π orbitals.[21] The Soret bands of the Pd complexes (around 300–360 nm) also shift to the higher energy side compared with the corresponding zinc complexes (360–390 nm). In addition, broad absorption bands appear between the Soret and Q bands (400–500 nm). Intense dispersion-type MCD signals corresponding to these broad absorption bands suggest degeneracy in the excited states. As has been reported previously, these bands may originate from metal-to-ligand charge-transfer transition ($d_\pi\rightarrow\pi^*$).[21]

Luminescence spectra: Luminescence measurements were made at 77 K to determine the excited state energies. Figure 4 shows the luminescence spectra of the zinc complexes, and data are summarized in Table 3. In the fluorescence of the zinc complexes (600–800 nm), the small Stokes shift is characteristic of robust, rigid Pc derivatives. Indeed, two vibronic bands whose vibrational spacings are 600–730 and 1350–1480 cm^{-1} are detected. These vibrational energies are close to those observed in the electronic absorption spectra and thus support the band assignments. In the near IR region (900–1300 nm), phosphorescence of all zinc complexes is observed with a weak vibronic band (vibrational

Table 3. Luminescence data at 77 K.

Compd	λ_F [nm][a]	λ_P [nm][a]	ΔE_{ST} [cm^{-1}][b]
0Zn	641	932	4900
1Zn	671	999	4900
2AdZn	660	987	5100
2OpZn	712	1106	5000
3Zn	689	1084	5300
4Zn	676	1122	5900
1Pd	–	927	–
2AdPd	–	929	–
2OpPd	–	1012	–
3Pd	–	1001	–

[a] λ_F and λ_P denote fluorescence and phosphorescence maxima. [b] Energy difference between fluorescence and phosphorescence peaks.

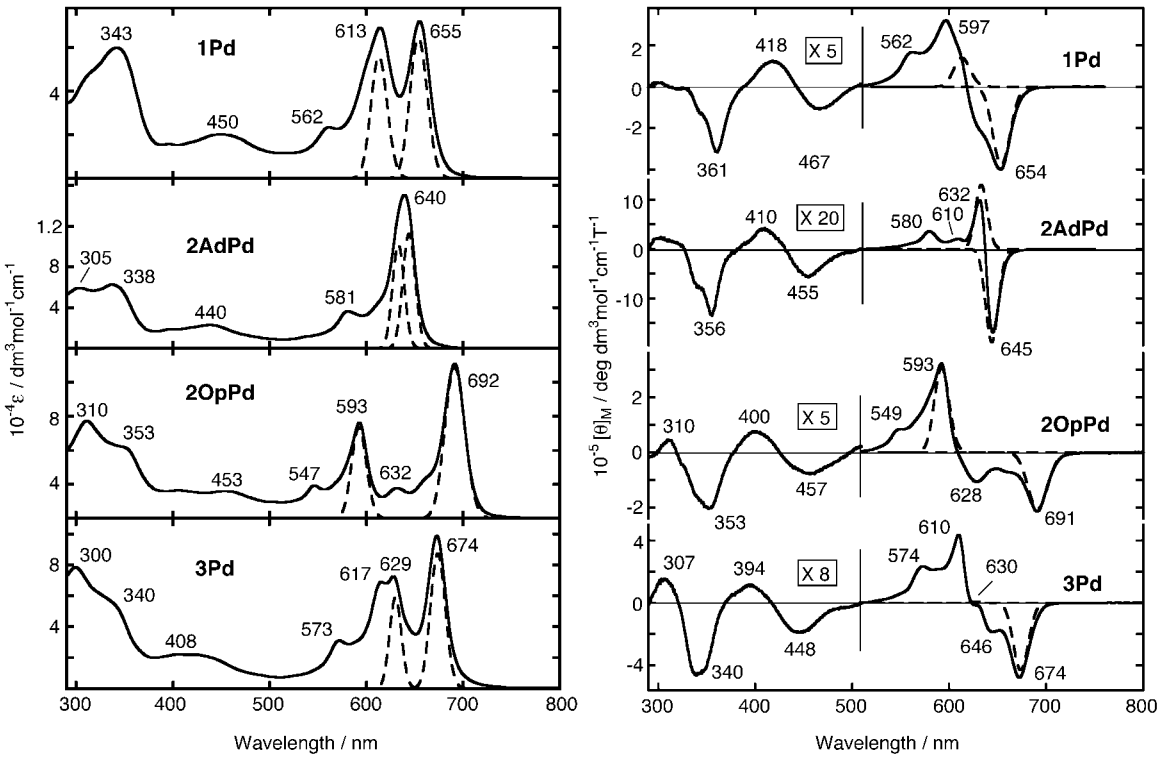

Figure 3. Electronic absorption (left) and MCD (right) spectra of the palladium complexes recorded in toluene/$CHCl_3$ (1/1). The Q_x and Q_y bands evaluated by band-deconvolution analyses are also shown (broken lines).

energy ca. 700 cm^{-1}). The T_{1x} energy decreases in the order **0Zn** (932 nm, 1.07×10^4 cm^{-1}) > **2AdZn** (987 nm, 1.01×10^4 cm^{-1}) > **1Zn** (999 nm, 1.00×10^4 cm^{-1}) > **3Zn** (1084 nm, 9.23×10^3 cm^{-1}) > **2OpZn** (1106 nm, 9.04×10^3 cm^{-1}) > **4Zn** (1122 nm, 8.91×10^3 cm^{-1}). This order is the same as that of the ΔE_{o-r} values, with the exception of **4Zn**, that is, the Coulomb integral between the HOMO and LUMO electrons is relatively large for **4Zn**. The energy difference between the S_{1x} and T_{1x} states ΔE_{ST}, which originates mainly from the exchange integral between the HOMO and LUMO electrons, was evaluated from the fluorescence and phosphorescence peaks. The ΔE_{ST} value increases in the order **0Zn** (4900 cm^{-1}) ≈ **1Zn** (4900 cm^{-1}) < **2OpZn** (5000 cm^{-1}) < **2AdZn** (5100 cm^{-1}) < **3Zn** (5300 cm^{-1}) < **4Zn** (5900 cm^{-1}). Since the ΔE_{ST} values of unsubstituted ZnTAP and ZnPc are 5400–6000 cm^{-1},[8,22] the relatively small ΔE_{ST} value for **0Zn** may originate from the phenyl groups. As a result, the ΔE_{ST} value of **4Zn** is largest in these Zn complexes, which is consistent with the large Coulomb integral. For the Pd complexes, only phosphorescence peaks were observed (Table 3), which were shifted to the higher energy side compared with the corresponding Zn complexes by 700–800 cm^{-1}, similar to the electronic absorption spectra.

Time-resolved EPR: TREPR measurements were carried out for the Zn and Pd complexes to obtain information on the electronic structures in the T_{1x} state. TREPR spectra of the zinc complexes are shown in Figure 5, and the zero-field splitting (zfs) parameters D and E, and sublevel population ratios used in the spectral simulations are summarized in Table 4. These spectra exhibit an AAA/EEE polarization pattern, which is reproduced by selective intersystem crossing (ISC) to the z sublevel of the T_{1x} state. Here, the E and A polarizations denote emission and absorption of microwaves, respectively, and originate from nonequilibrium population in the triplet sublevels. This selectivity originates from the z component of SOC between the d_{xz} and d_{yz} orbitals of the zinc atom, which are admixed with the LUMOs of the ligand.[8,23]

Table 4. Observed EPR parameters D_{obsd}, E_{obs}, and g_{zz} with sublevel population ratios P_y:P_x:P_z and calculated zfs parameters D_{calcd} and E_{calcd}.

Compd	D [10^{-3} cm^{-1}]	D_{calcd} [10^{-3} cm^{-1}]	$\lvert E\rvert$ [10^{-3} cm^{-1}]	$\lvert E_{calcd}\rvert$ [10^{-3} cm^{-1}]	g_{zz}	P_y:P_x:P_z
0Zn	29.0	28.0	5.33	3.20[a] (13.0[b])	1.999	0.1:0:0.9
1Zn	26.0	25.5	4.00	3.80	1.999	0.2:0:0.8
2AdZn	26.8	26.5	8.54	10.8	1.998	0:0.4:0.6
2OpZn	23.5	21.3	5.17	4.76	1.999	0.2:0:0.8
3Zn	22.8	21.3	2.92	4.49	1.999	0.2:0:0.8
4Zn	21.8	21.1	6.09	4.26[a](7.96[b])	1.995	0:0:1
1Pd	−221	–	5.00	–	1.968	0.1:0:0.9
2OpPd	−141	–	0	–	1.985	0:0:1
3Pd	−215	–	0	–	1.971	0:0:1

[a] E values calculated by using the e_{gy} orbital shown in Figure 9. [b] E values calculated by using the linear combination of the e_{gx} and e_{gy} orbitals as the LUMO, whose nodes lie along the *meso–meso* direction.

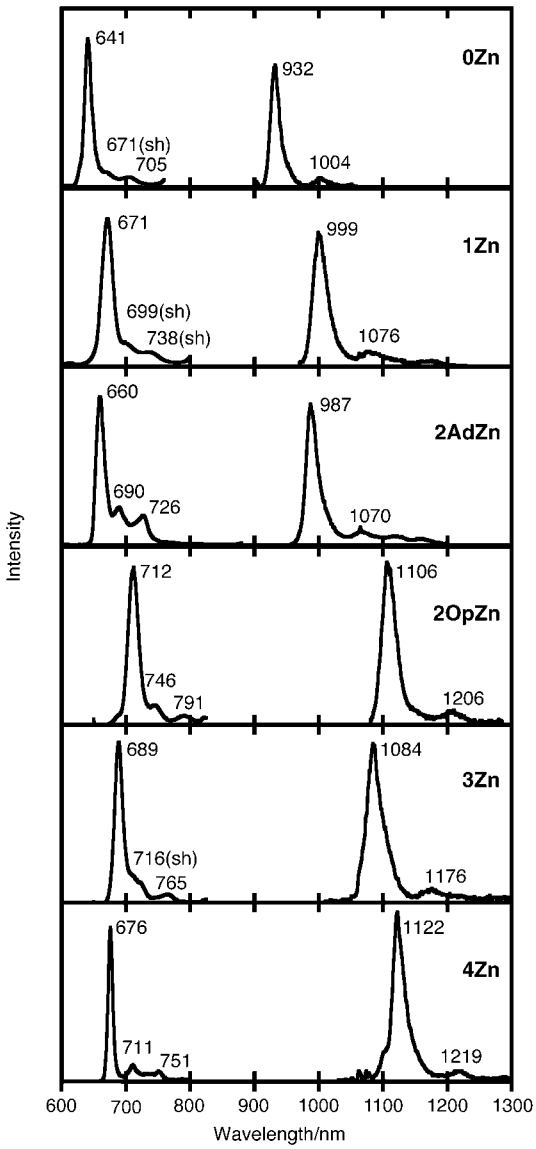

Figure 4. Luminescence spectra of the zinc complexes in toluene containing 1×10^{-2} M pyridine at 77 K.

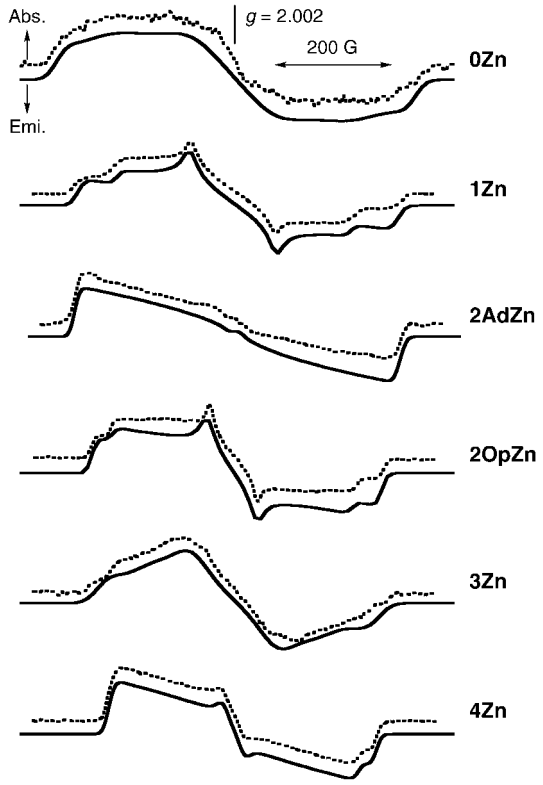

Figure 5. TREPR spectra (dotted lines) of the zinc complexes in cyclohexanol (toluene containing 0.1 M pyridine was used for **4Zn**) together with their simulations (solid lines). These spectra were observed at 20 K and 1 μs after laser excitation.

The zfs of Pc and TAP complexes originates from the magnetic dipole–dipole interaction between the HOMO and LUMO electrons, and spin–orbit interaction between the T_{1x} and T_{1y} states. Since the deviation of the observed g_{zz} value, Δg_{zz} ($=g_{zz}-2.0023$), is negligibly small (<0.006), it is considered that the observed zfs is little influenced by the SOC between the T_{1x} and T_{1y} states, and therefore reflects the magnetic dipole–dipole interaction.[8,23] The D value, which reflects the anisotropic interaction between unpaired electrons towards the out-of-plane axis (z), decreases in the order **0Zn** (2.90×10^{-2} cm^{-1}) > **1Zn** (2.60×10^{-2} cm^{-1}) > **2OpZn** (2.35×10^{-2} cm^{-1}) > **3Zn** (2.28×10^{-2} cm^{-1}) > **4Zn** (2.18×10^{-2} cm^{-1}) with expansion of the π-conjugated systems, except for **2AdZn** (2.68×10^{-2} cm^{-1}). This indicates that the π electron is delocalized over the fused benzo rings in the T_1 state. The relatively large D value of **2AdZn** is qualitatively interpreted in terms of the π-electron distribution. Since the MO calculations indicate that the π-electron density on the pyrrole rings without fused benzo rings is larger than that on the benzo-fused pyrrole rings, the magnetic dipole–dipole interaction between unpaired π electrons is larger for adjacent pyrrole rings than for opposite pyrrole rings.[24,25] To allow a quantitative discussion, the zfs due to the magnetic dipole–dipole interaction between the HOMO and LUMO electrons was calculated under the half-point charge approximation (Table 4).[24,26] Indeed, the calculated D values reproduce the experimental trends nicely.

On the other hand, the $|E|$ value, which reflects the anisotropic interaction between unpaired electrons towards the in-plane axes (x and y), decreases in the order **2AdZn** (8.54×10^{-3} cm^{-1}) > **4Zn** (6.09×10^{-3} cm^{-1}) > **0Zn** (5.33×10^{-3} cm^{-1}) > **2OpZn** (5.17×10^{-3} cm^{-1}) > **1Zn** (4.00×10^{-3} cm^{-1}) > **3Zn** (2.92×10^{-3} cm^{-1}), without having any correlation with the D value. The large $|E|$ value of **4Zn** with D_{4h} symmetry is interpreted in terms of the Jahn–Teller effect. Langhoff et al. have shown that the $|E|$ value of porphyrins is largest when the nodes lie along the *meso–meso* direction.[27] In fact, the T_1 optimum structure of ZnPc calculated using the ZINDO/1 Hamiltonian indicates that the nodes of the LUMO lie along the *meso–meso* direction, and that the Jahn–Teller structural distortion is very small (distances between the *meso–meso* nitrogen atoms differ by ca. 0.06 Å between the x' and y' axes). In a similar manner, the largest $|E|$ value of **2AdZn** originates from the nodes of the LUMO along the *meso–meso* direction. These experimental trends are well reproduced by the half-point charge calculations (Table 4).[24,26]

It is noteworthy that the D value of **2AdZn** decreases with increasing temperature ($D(20\,\mathrm{K}) = 2.68\times10^{-2}\,\mathrm{cm}^{-1} \rightarrow D(250\,\mathrm{K}) = 2.60\times10^{-2}\,\mathrm{cm}^{-1}$, Figure 6) without a significant change in the $|E|$ value,[28] while this kind of temperature dependence is not seen for **1Zn** and **2OpZn** (for **0Zn** and **3Zn**, no TREPR signal was observed at high temperature). This decrease in D value is reasonably interpreted as due to a change in the population between the T_{1x} and nearby T_{1y} states, since the half-point charge calculations indicate that the calculated D value of the T_{1y} state ($2.41\times10^{-2}\,\mathrm{cm}^{-1}$, the HOMO–LUMO+1 configuration) is smaller than that of the T_{1x} state ($2.65\times10^{-2}\,\mathrm{cm}^{-1}$, the HOMO–LUMO configuration).[26] In this case, the observed D value D_{obsd} is represented by Equation (1).[29]

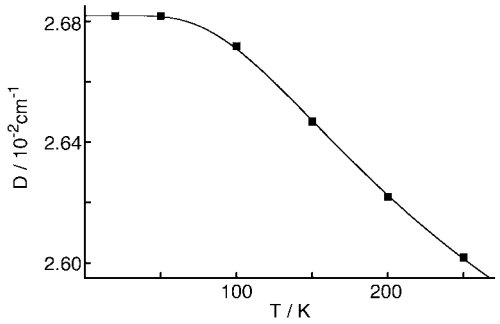

Figure 6. Temperature dependence of the D values of **2AdZn**. The change in the D value was reproduced using Equation (1) (solid line).

$$D_{\mathrm{obsd}}(\mathbf{2AdZn}) = \{D(\mathrm{T}_{1x})P_1 + D(\mathrm{T}_{1y})P_2\}/(P_1 + P_2) \quad (1a)$$

$$P_1 = \exp(\Delta E_{\mathrm{TT}}/2\,kT),\ P_2 = \exp(-\Delta E_{\mathrm{TT}}/2\,kT) \quad (1b)$$

Here, $D(\mathrm{T}_{1x})$ was reasonably assumed as the D value at 20 K. The changes in D_{obsd} were well reproduced by using Equation (1) (solid line in Figure 6), from which the ΔE_{TT} and $D(\mathrm{T}_{1y})$ values were evaluated as 2.5×10^{2} and $2.30\times10^{-2}\,\mathrm{cm}^{-1}$, respectively. Thus, the T_{1y} energy of **2AdZn** is very close to the T_{1x} energy, similar to the S_{1x} and S_{1y} states.

Of the Pd complexes, TREPR signals were detected for **1Pd**, **2OpPd**, and **3Pd** (Figure 7),[30] while no TREPR signal could be observed for **2AdPd**. These TREPR spectra exhibit an EEEE/AAA polarization pattern, where the intense E signal at the lowest magnetic field is assigned to the $\Delta m_s = 2$ transition, while the other signals correspond to the $\Delta m_s = 1$ transitions. Although these spectra are reproduced by selective ISC to the z sublevel of the T_{1x} state, similarly to the Zn complexes, the $|D|$ and Δg_{zz} values of the Pd complexes are much larger than those of the Zn complexes (Table 4). These EPR parameters are characteristic of porphyrinic complexes with an open-shell atom[31–33] and originate from the z component of SOC between the T_{1x} and T_{1y} states, reflecting the ΔE_{TT} value. It has been shown that the zfs of PdPc and Pd porphyrin complexes with a small ΔE_{TT} value is too large to be observed by X-band EPR (ca. $0.3\,\mathrm{cm}^{-1}$).[31,32] Indeed, since the experimentally obtained ΔE_{TT} value of **2AdZn** is very small, the absence of a TREPR signal for **2AdPd** can be interpreted by the large zfs (outside range of X-band EPR). The $|D|$ and Δg_{zz} values increase in the order **2OpPd** < **1Pd** < **3Pd**, in contrast to the ΔE_{SS} value. The D values of the Pd complexes are analyzed in terms of the ΔE_{TT} value below.

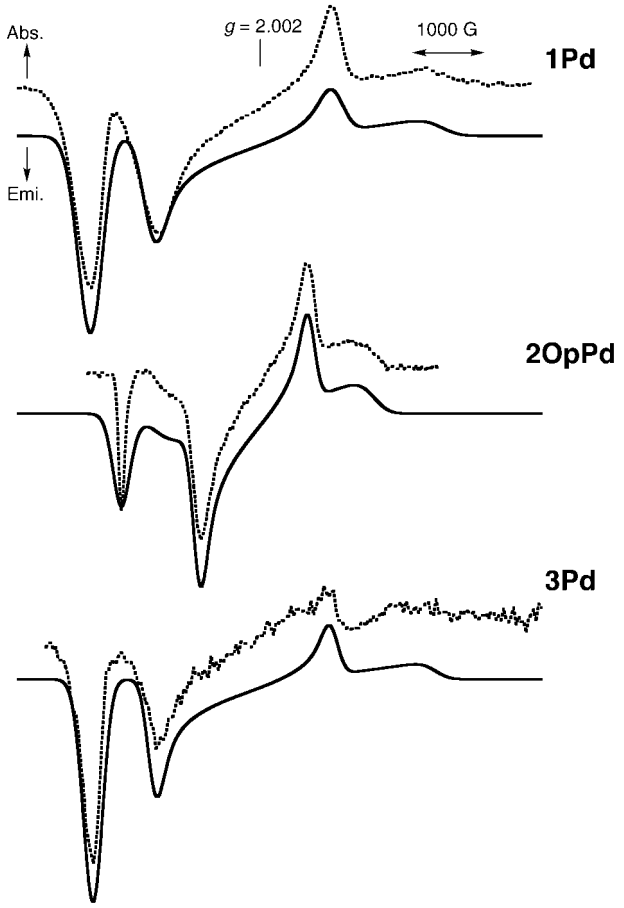

Figure 7. TREPR spectra (dotted lines) of the palladium complexes in toluene/$CHCl_3$ (1/1) together with their simulations (solid lines). The spectra were observed at 10 K and 0.7 μs after laser excitation.

Discussion

Electronic structures of frontier orbitals: In this section, the relationship between frontier orbitals and π-conjugated systems is discussed in terms of the CV results and MO calculations.

The first oxidation potential shifts to negative potentials in the order **0Zn** > **1Zn** > **2AdZn** ≈ **2OpZn** > **3Zn** > **4Zn**. The difference in the first oxidation couple between **2AdZn** and **2OpZn** of only 0.02 V indicates that the potential shift depends only on the size of the π-conjugated system, and that the HOMO is destabilized by expansion of the π system. On the other hand, the first reduction potential shifts to negative values in the order **0Zn** ≈ **1Zn** ≈ **2OpZn** > **2AdZn** ≈ **3Zn** > **4Zn**. In contrast to the HOMO, since the LUMO energy appears to have no dependence on the number of fused benzo rings, it is necessary to clarify the relationship between the LUMO energy and the π-conjugated system.

Accordingly, to characterize the frontier orbitals quantitatively, MO calculations were carried out with the PPP, PM3, and ZINDO/S methods.[24,25] Since the results of these calculations were similar in terms of the effects of the fused benzo rings on the TAP skeleton, we will discuss the expansion of π-conjugated system using the typical MO energies and frontier orbitals calculated within the framework of the PPP method (Figure 8a and Figure 9). The HOMO becomes energetically destabilized with increasing size of the π-conjugated system, which is consistent with the CV results (Figure 8b). On the other hand, destabilization of the LUMO and LUMO+1 depends on the symmetry of the π-conjugated system, and the variation in the LUMO energy elegantly resembles that seen for the first reduction potential in the CV measurements (Figure 8b). The behavior of the MO energies will now be discussed in terms of the electron distribution of MOs.

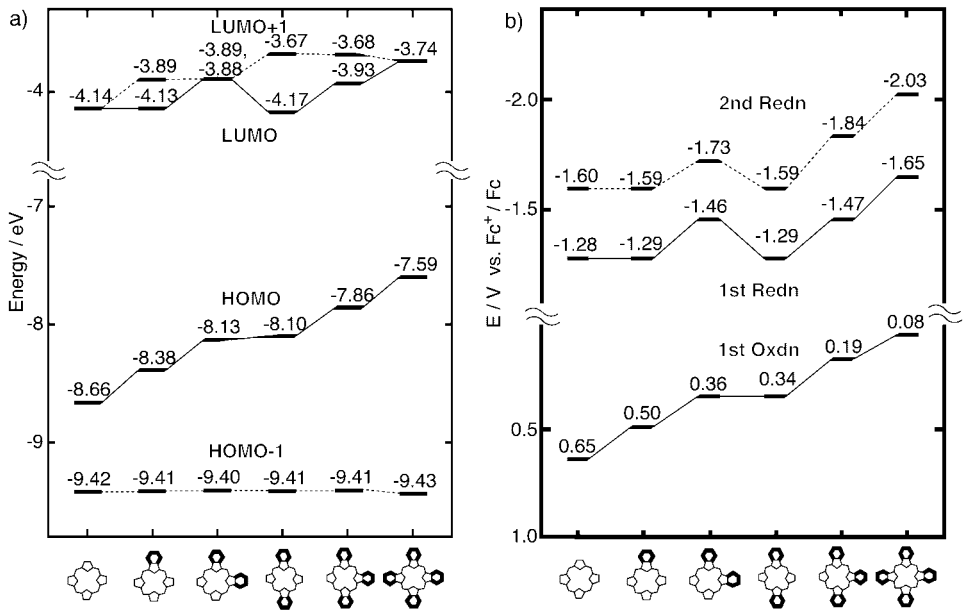

Figure 8. Calculated energies of the four frontier orbitals (a) and electrochemical data (b) of the zinc compounds in this study, recorded at a scan rate of 50 mV s^{-1} in *o*-DCB containing 2.5×10^{-2} M pyridine and 0.1 M TBAP.

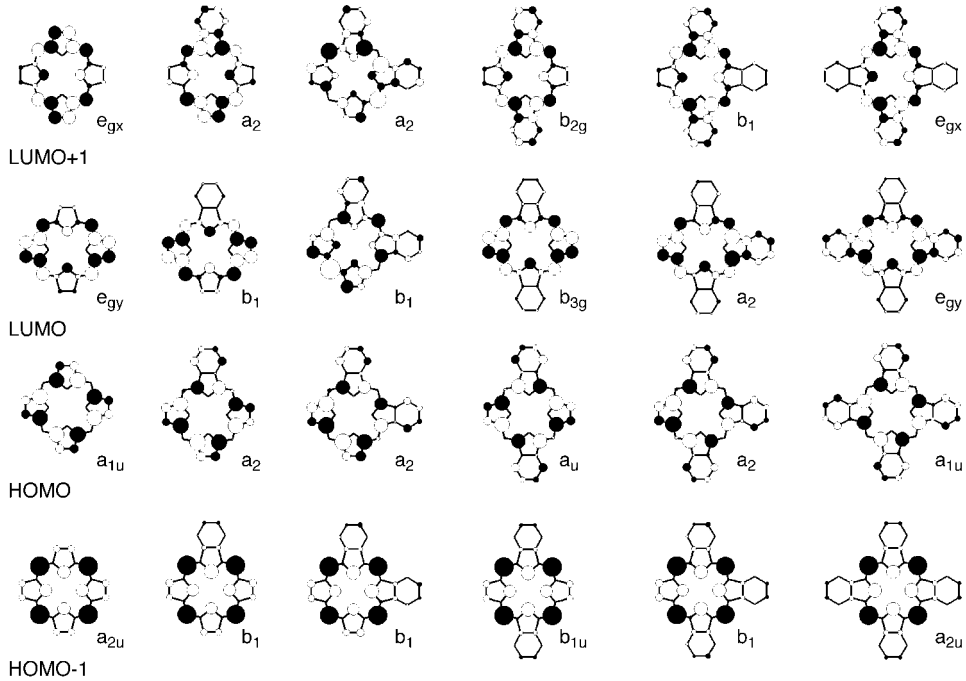

Figure 9. Four frontier orbitals of low-symmetry TAP derivatives. In the cases of D_{4h}-type TAP and Pc (extreme left- and right-hand sides, respectively), the LUMO and LUMO+1 are degenerate.

In the case of the HOMO of **0Zn**, since the electron densities at the C_β positions of the pyrrole rings are large, the HOMO is destabilized by fused benzo rings. In addition, the electron distributions at the C_β positions are independent of the pyrrole rings for **0Zn**. Therefore, the HOMO destabilization due to the fused benzo rings is independent of the pyrrole ring to which the benzo group is fused, and exhibits a good relationship with the size of the π-conjugated system.

On the other hand, the behavior of the LUMOs e_{gx} and e_{gy} is complex because of the degeneracy. In the e_{gx} (or e_{gy}) orbital, the electron densities at the C_β positions are larger in the pyrrole rings on the *y* (*x*) axis than those on the *x* (*y*) axis. Therefore, the effect of fused benzo rings on the *x* axis is different from that on the *y* axis. For example, in **1Zn**, in which the benzo ring is fused on the *y* axis of **0Zn**, only the e_{gx} orbital, which becomes the LUMO+1, is destabilized, while no change occurs in the energy of e_{gy}, which becomes the LUMO, and this results in energy splitting between the LUMO and LUMO+1 (Figure 10). Addition of a benzo ring to **1Zn** results in two isomers, **2OpZn** and **2AdZn**. In the former, the second benzo ring is also fused on the *y* axis. Therefore, only the LUMO+1 energy is destabilized, while the LUMO energy is essentially not influenced by the fused benzo ring (Figure 10). On the other hand, since the second benzo ring is fused on the *x* axis, the effect on **2AdZn** is clearly dif-

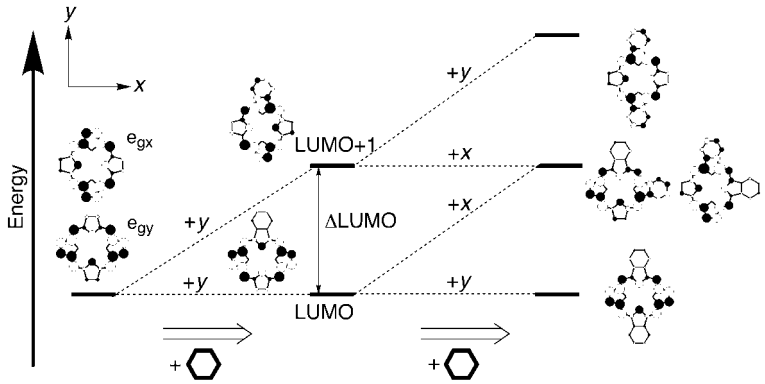

Figure 10. Effects of fused benzo rings on the LUMO and LUMO+1 energies.

ferent from that on **2OpZn**.[34] Compared with **1Zn**, the LUMO originating from the e_{gy} orbital of **0Zn** is destabilized, while the LUMO+1 originating from the e_{gx} orbital of **0Zn** is hardly influenced. Thus, the LUMO energy is very close to the LUMO+1 energy for **2AdZn** (Figure 10). From the viewpoint of the **0Zn**→**2AdZn** transformation, benzo rings are fused on both the *x* and *y* axes, so that the e_{gx} and e_{gy} orbitals are destabilized to a similar extent. This appears to be the reason why the LUMOs, S_1, and T_1 states of **2AdZn** are almost degenerate in spite of the C_{2v} molecular symmetry. In the case of **3Zn**, the destabilization of the LUMO+1 is twice that of the LUMO, because one and two benzo rings are fused on the *x* and *y* axes, respectively. For **4Zn**, the LUMOs are degenerate due to the D_{4h} symmetry. Consequently, the effects of fused benzo rings on the degenerate LUMO energies of **0Zn** are reasonably explained.

By using this model, the destabilization of the HOMO and LUMO levels can be evaluated from the CV results. In the case of the first oxidation potential, the potential shift is approximately proportional to the number of fused benzo rings (ca. 0.14 V per benzo unit, dotted line in Figure 11), which reflects the destabilization of the HOMO. The first reduction potential only shifts when the benzo ring is fused on the *x* axis, that is, in the transformations of **1Zn**→**2AdZn**, **2OpZn**→**3Zn**, and **3Zn**→**4Zn**. The fact that the first reduction potentials of **0Zn**, **1Zn**, and **2OpZn** are almost identical, while those of **2AdZn** and **3Zn** are also very close to each other, indicates that this model is appropriate. The shift in reduction potential is closely proportional to the number of fused benzo rings on the *x* axis (ca. 0.18 V per benzo unit, broken line in Figure 11), which corresponds to the destabilization of the LUMO.

The destabilization of the LUMO (ca. 0.18 V per benzo unit) is larger than that of the HOMO (ca. 0.14 V per benzo unit), while the S_{1x} and T_{1x} energies, consisting of the HOMO→LUMO configuration, shift to lower energy for the **0Zn**→**4Zn** transformation. This is reasonably interpreted by the degeneracy of the LUMOs. While the a_{1u} orbital energy destabilizes due to the four fused benzo rings, the e_{gx} and e_{gy} orbital energies are destabilized by only two benzo rings fused on the *y* and *x* axes (in other words, the effect on the e_g orbitals is dispersed since they are degenerate), respectively, leading to the red shift of the S_1 and T_1 energies.

Since, as described above, the destabilization energies of the LUMOs were evaluated from the shift of the first reduction potential, we attempted to evaluate the ΔLUMO values experimentally. First, it is reasonable to assume that the LUMO and LUMO+1 energies are destabilized by fusing benzo rings on the *x* and *y* axes, respectively. Accordingly, the ΔLUMO value is expressed as $1500\,(N_y - N_x)\ \mathrm{cm}^{-1}$, where N_y and N_x denote the number of fused benzo rings on the *y* and *x* axes, respectively. Consequently, the ΔLUMO values were evaluated as 3000, 1500, and 1500 cm^{-1} for **2OpZn**, **1Zn**, and **3Zn**, respectively, while the LUMOs were degenerate in the case of **0Zn**, **2AdZn**, and **4Zn**. The ΔLUMO values exhibit a good relationship with the ΔE_{SS} values. While some electronic effects of fused benzo rings have already been reported in terms of CV measurements and MO calculations,[9–13] these studies focused mainly on the size of the π-conjugated system under the same symmetry. Therefore, the present study is the first experimental demonstration of the electronic relationship between fused benzo rings and MO energies.

Excited singlet states: To quantitatively examine the electronic absorption spectra of the zinc complexes, CI calculations were performed with the ZINDO/S Hamiltonian.[25] Calculated spectra are shown in Figure 12, and the calcula-

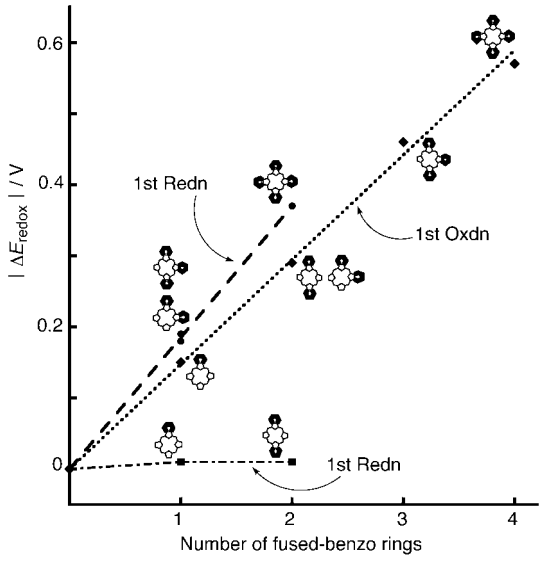

Figure 11. Relationships between the redox potentials (◆: first oxidation, ● and ■: first reduction) and number of fused benzo rings. The ΔE_{redox} values denote the difference in the first oxidation or reduction potential between **0Zn** and the other Zn complexes. The ● and ■ data correspond to the number of benzo rings fused on the *x* and *y* axes, respectively. The first reduction potentials of **1Zn** and **2OpZn** are similar to that of **0Zn**, while those of **2AdZn**, **3Zn**, and **4Zn** shift to negative values.

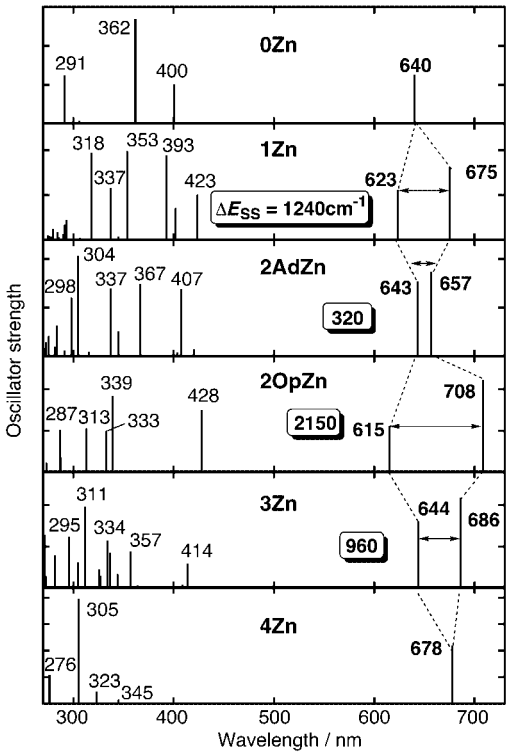

Figure 12. Absorption wavelengths and oscillator strengths obtained by CI calculations on the zinc complexes.

tion results, including direction of transition dipoles and configurations, are summarized in Table 5. While the Q band of **0Zn** and **4Zn** consists of degenerate transitions, the Q bands of the low-symmetry TAP derivatives split, with the energy splitting decreasing in the order **2OpZn** > **1Zn** > **3Zn** > **2AdZn**. Furthermore, the Q_x band shifts to lower energy in the order **0Zn** > **2AdZn** > **1Zn** > **4Zn** > **3Zn** > **2OpZn**. These experimental trends in the Q band regions are reproduced sufficiently by the CI calculations, while there are too many transitions in the Soret-band region for quantitative interpretations.[17] The main electronic properties obtained from the calculations are as follows. 1) The transition dipole moments of Q_x and Q_y bands are orthogonal to each other, and lie along the short (x) and long (y) axes, respectively. 2) The Q bands consist mainly of the HOMO→LUMO (or LUMO+1) (>85%) and HOMO−1→LUMO+1 (or LUMO) configurations, which is consistent with the good relationships between the ΔE_{o-r} and S_{1x} energies, and between the ΔE_{SS} and ΔLUMO values. 3) The oscillator strength of the Q_y band is smaller than that of the Q_x band. This is reasonably interpreted by the fact that the configuration interaction is larger in the Q_y band (HOMO→LUMO+1 and HOMO−1→LUMO) than in the Q_x band (HOMO→LUMO and HOMO−1→LUMO+1) because of the smaller energy difference in the former.

Excited triplet states: The $|D|$ values of the Pd complexes are much larger than those of the Zn complexes. These large $|D|$ values are characteristic of the z component of a large SOC between the T_{1x} and T_{1y} states.[31–33] In this section, we evaluate the ΔE_{TT} values quantitatively. The observed D value D_{obsd} is represented by Equation (2), where D_{SS} and D_{SOC} denote D values due to the magnetic dipole–dipole interaction and SOC, respectively.

$$D_{obsd}(Pd) = D_{SS} + D_{SOC} \quad (2)$$

By using D values of the Zn complexes as the D_{SS} values, D_{SOC} values $[=D_{obsd}(Pd)-D_{obsd}(Zn)]$ were evaluated as −0.247, −0.166, −0.238 cm^{-1} for **1Pd**, **2OpPd**, and **3Pd**, respectively. Under the second-order perturbation theory, the D_{SOC} is expressed as Equation (3),[29] where Z is a matrix element of the SOC, related to both the SOC constant (ξ = 1610 cm^{-1}) and the LUMO (LUMO+1) coefficients of d_{yz} (d_{xz}) orbitals of the Pd atom, C_{dyz} (C_{dxz}).[35]

$$D_{SOC} = -Z^2/4\Delta E_{TT} \quad (3a)$$

$$iZ = \xi C_{dyz} C_{dxz} \langle d_{yz}|l_z|d_{xz}\rangle \quad (3b)$$

The Z values have been experimentally evaluated as 24±5 and 33±4 cm^{-1} for Pd porphyrin and PdPc complexes, respectively.[31,32] Since the extended Hückel MO calculations indicated that the Z value is hardly dependent on the size and type of π-conjugated systems,[36] their average value (29±5 cm^{-1}) was employed for our complexes. Thus, the ΔE_{TT} values were experimentally evaluated as 850±300, 1300±400, and 880±300 cm^{-1} for **1Pd**, **2OpPd**, and **3Pd**, respectively, and are therefore much larger than that of **2AdZn** (250 cm^{-1}). These ΔE_{TT} values exhibit a good parallel relationship with the ΔLUMO and ΔE_{SS} values, as summarized in Figure 13.

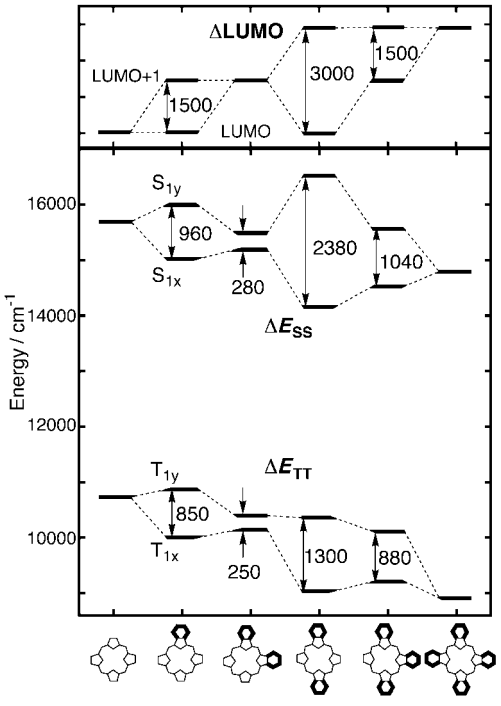

Figure 13. Summary of the ΔLUMO, ΔE_{SS}, and ΔE_{TT} values.

Table 5. Calculated transition energies, oscillator strengths f, and configurations of the zinc complexes.

Compd	λ [nm]	$\tilde{\nu}$ [cm^{-1}]	f	Polarization[a]	Configuration[b,c]		
0Zn	640	15630	0.63		169→170 (85)	168→171 (9)	
	640	15630	0.63		169→171 (85)	168→170 (9)	
	400	24980	0.512		165→170 (38)	168→170 (19)	165→171 (18)
	400	24980	0.510		165→171 (38)	168→171 (19)	165→17 0 (18)
	362	27650	1.349		168→171 (46)	165→171 (21)	168→170 (13)
	362	27650	1.348		168→170 (46)	165→170 (21)	168→171 (13)
	291	34350	0.624		169→174 (54)	157→170 (12)	157→171 (10)
	291	34350	0.622		169→175 (54)	157→170 (10)	157→171 (12)
	269	37200	0.140		169→175 (23)	157→170 (20)	
	269	37200	0.143		169→174 (23)	157→171 (21)	
1Zn	675	14810	0.814	x	162→163 (89)	161→164 (6)	
	623	16050	0.558	y	162→164 (85)	161→163 (9)	
	423	23620	0.505	y	160→163 (62)	161→163 (12)	159→165 (6)
	402	24890	0.356	x	161→164 (44)	160→164 (36)	161→165 (5)
	393	25480	0.944	y	161→163 (70)	160→163 (19)	162→164 (5)
	354	28290	0.991	x	161→164 (37)	160→164 (44)	158→164 (5)
	337	29690	0.582	x	158→164 (60)	162→166 (16)	158→165 (10)
	318	31460	0.973	y	158→163 (76)	162→167 (5)	158→166 (5)
	293	34130	0.222	y	162→167 (42)		
	291	34330	0.170	x	162→168 (65)		
	280	35750	0.123	y	162→167 (30)	151→163 (23)	
2AdZn	657	15230	0.867	x'	155→156 (89)	154→157 (5)	
	643	15550	0.772	y'	155→157 (90)	154→156 (5)	
	407	24560	0.693	y'	154→156 (69)	153→157 (14)	154→158 (5)
	367	27270	0.223	y'	153→157 (74)	154→156 (16)	
	367	27280	0.746	x'	154→157 (74)	153→156 (12)	152→157 (4)
	345	28990	0.258	y'	155→159 (62)	151→157 (21)	
	337	29690	0.698	x'	152→157 (49)	151→156 (22)	155→160 (6)
	305	32830	1.031	y'	155→161 (41)	152→156 (35)	151→157 (6)
	298	33590	0.604	x'	152→157 (23)	151→156 (48)	
	283	35310	0.313	x'	155→162 (34)	155→164 (21)	144→157 (26)
	275	36320	0.208	y'	146→156 (24)		
2OpZn	708	14120	1.113	x	155→156 (91)	154→157 (3)	
	615	16270	0.557	y	155→157 (85)	154→156 (10)	
	428	23380	0.751	y	154→156 (74)	152→156 (9)	155→157 (6)
	339	29520	0.918	x	154→157 (81)	152→157 (10)	
	333	30030	1.679	y	152→156 (80)	154→156 (8)	155→157 (4)
	332	30080	0.497	x	155→160 (75)	152→157 (15)	154→157 (3)
	313	32000	0.530	x	155→160 (21)	152→157 (52)	151→158 (8)
	287	34800	0.180	y	155→162 (59)	155→164 (28)	
	287	34900	0.511	x	145→156 (46)	155→169 (13)	153→158 (8)
	273	36660	0.115	y	155→166 (37)		
3Zn	686	14580	1.085	x	148→149 (92)		
	644	15540	0.806	y	148→150 (90)	147→149 (4)	
	414	24170	0.297	y	147→149 (83)		
	357	28030	0.442	x	147→150 (86)	146→150 (5)	
	344	29080	0.168	y	144→149 (72)		
	337	29720	0.426	x	148→154 (68)	146→150 (15)	
	334	29970	0.570	y	145→150 (49)	146→149 (26)	148→152 (7)
	327	30630	0.152	x	148→154 (24)	146→150 (24)	145→149 (33)
	325	30730	0.229	y	148→153 (77)		
	311	32130	0.980	y	146→149 (44)	145→150 (31)	148→153 (5)
	304	32840	0.314	x	146→150 (27)	145→149 (40)	
	295	33870	0.616	x	148→155 (21)	144→150 (37)	144→152 (8)
	281	35560	0.394	y	148→157 (37)	138→149 (21)	
	273	36700	0.142	x	142→149 (27)	134→149 (34)	
	272	36830	0.641	x	144→150 (19)	142→149 (7)	
4Zn	678	14760	1.096		141→142 (91)	140→143 (4)	
	678	14760	1.096		141→143 (91)	140→142 (4)	
	323	30960	0.227		137→142 (52)	140→142 (22)	141→146 (10)
	323	30960	0.227		137→143 (52)	140→143 (22)	141→147 (10)
	305	32780	1.973		140→142 (59)	137→142 (22)	139→145 (6)
	305	32780	1.973		140→143 (59)	137→143 (22)	138→145 (6)
	276	36230	0.546		141→150 (52)	133→142 (17)	134→143 (8)
	276	36230	0.546		141→151 (52)	133→143 (17)	134→142 (8)

[a] For **2AdZn**, the x' and y' axes lie along the *meso–meso* direction and are short and long axes, respectively. [b] Percentage contribution of the configuration is given in parentheses. [c] **0Zn** (HOMO = 169), **1Zn** (HOMO = 162), **2AdZn** (HOMO = 155), **2OpZn** (HOMO = 155), **3Zn** (HOMO = 148), **4Zn** (HOMO = 141).

Conclusion

We have prepared a series of TAP derivatives with various π-conjugated systems by fusing benzo rings and quantitatively characterized the electronic structures. The ΔLUMO, ΔE_{SS}, and ΔE_{TT} values were found to have a parallel relationship. The shift of the first oxidation and reduction potentials, and the relationship between the frontier orbitals and fused benzo rings were quantitatively characterized in terms of the CV measurements and MO calculations. In particular, the ΔLUMO values were evaluated experimentally for the first time and could be reasonably explained by using the magnitude of the MO coefficients. In the S_1 states, the ΔE_{SS} values were estimated from electronic absorption and MCD spectra, and MO calculations succeeded in reproducing the experimental trend. In the T_1 states, it was shown that the ΔE_{TT} values can be evaluated by analyzing the temperature dependence of the zfs and SOC of the Pd complexes. These methods for evaluating the molecular properties are useful not only for understanding the porphyrin and Pc complexes, but also for preparing novel functional molecules.

Experimental Section

Instrumental techniques: Electronic absorption spectra were measured with a Hitachi U-3410 spectrophotometer. MCD measurements were made with a JASCO J-720 spectrodichrometer equipped with a JASCO electromagnet producing magnetic fields of up to 1.09 T with parallel and antiparallel fields. Fluorescence spectra were recorded with a Hitachi F-4500 spectrofluorimeter. Near-IR phosphorescence measurements were performed with a monochromator (JASCO CT-25CP) and a photomultiplier (Hamamatsu Photonics R5509-42), which was cooled at 193 K by a cold nitrogen gas flow system (Hamamatsu Photonics R6544-20).[37] The photon signals, amplified by a fast preamplifier (Stanford

Research SR445), were measured by the single-photon counting method using a photon counter (Stanford Research SR400). Samples were excited by an Nd:YAG laser (Spectra Physics INDI-30; 355 nm; 7 ns fwhm). Toluene of spectral grade containing pyridine and a 1:1 mixture of toluene and chloroform of spectral grades were used as solvents for the Zn and Pd complexes, respectively.

TREPR measurements were carried out on a Bruker ESP 300E spectrometer.[38] An Oxford ESR 900 cold gas flow system was used for controlling the temperature. Samples were excited at 585 nm by a dye laser (Lumonics HD 500) pumped with an excimer laser (Lumonics EX 500) or at 532 nm by a Nd:YAG laser (Spectra Physics INDI-30). The TREPR signals from the EPR unit were integrated by a LeCroy 9450A oscilloscope. For TREPR measurements, cyclohexanol or toluene of spectral grade containing 0.1 M pyridine and a 1:1 mixture of toluene and chloroform of spectral grades were used as solvents for Zn and Pd complexes, respectively.

CV measurements were made under a dry nitrogen atmosphere using a Hokuto Denko HA-501 potentiostat/galvanostat connected to a Hokuto Denko HB-105 function generator. Differential pulse voltammetry experiments were performed with a Yanaco Model P-1100 electric analyzer. Conventional three-electrode cells were used, in which a glassy carbon electrode (area 0.07 cm^2) and a platinum wire were used as the working electrode and auxiliary electrode, respectively. The reference electrode (AgCl/Ag) was corrected for junction potentials by reference to the ferrocenium/ferrocene (Fc^+/Fc) couple. In an *o*-dichlorobenzene (*o*-DCB) solution containing 0.1 M tetrabutylammonium perchlorate (TBAP), the Fc^+/Fc couple was observed at approximately 0.51 ± 0.02 V vs AgCl/Ag.

Computational methods: MO calculations were carried out by using the PPP, PM3, or ZINDO/S methods.[24,25] The CI calculations were also performed with the ZINDO/S Hamiltonian by means of the program HyperChem. R.5.1.[25] For CI calculations, all singly excited configurations of up to 10 eV were included. Band deconvolution of the spectral data was carried out with the program SIMPFIT developed by Stillman et al.[19] The zfs in the T_1 state was calculated under a half-point charge approximation,[26] in which the HOMO and LUMO coefficients obtained by the PPP calculations were employed.[24] Simulations of the T_1 TREPR spectra were carried out by following the procedure already reported.[39]

Synthesis: All new low-symmetry TAPs in Scheme 1 were obtained by mixed condensation between two types of dinitrile. Yields of the TAP derivatives were calculated on the basis of the total nitrile mixture.

Octa-2,3,7,8,12,13,17,18-phenyl-5,10,15,20-tetraazaporphinato(2−)zinc(II)[40,41] (0Zn): A 1-pentanol solution (3 mL) containing diphenylmaleonitrile[40] (110 mg, 4.77×10^{-4} mol) and a small amount of lithium was refluxed for 1 h. After adding an excess of zinc acetate, the solution was refluxed for 30 min. The solvent was evaporated, the remaining mixture washed with methanol, and the residue purified by chromatography on alumina and silica gel with pyridine as eluent. Recrystallization from $CHCl_3$/ethanol gave **0Zn** as a dark green powder in 18% yield (21 mg). Elemental analysis (%) calcd for $C_{64}H_{40}N_8Zn$: C 77.92, H 4.09, N 11.36; found: C 77.74, H 4.40, N 11.14; ^{1}H NMR (400 MHz, $CDCl_3$ + 1% C_5D_5N): $\delta = 7.59$–7.50 (m, 24H; *m*-Ph, *p*-Ph), 8.39 ppm (dd, 16H; *o*-Ph).

[2^2,2^3-Dioctyloxybenzo[*b*]-7,8,12,13,17,18-hexaphenyl-5,10,15,20-tetraazaporphinato(2−)]zinc(II) (1Zn), **[2^2,2^3,7^2,7^3-tetraoctyloxydibenzo[*b*,*g*]-12,13,17,18-tetraphenyl-5,10,15,20-tetraazaporphinato(2−)]zinc(II) (2AdZn)**, **and [2^2,2^3,12^2,12^3-tetraoctyloxydibenzo[*b*,*l*]-7,8,17,18-tetraphenyl-5,10,15,20-tetraazaporphinato(2−)]zinc(II) (2OpZn)**: Diphenylmaleonitrile[40] (670 mg, 2.90×10^{-3} mol) and 4,5-dioctyloxyphthalonitrile[42] (609 mg, 1.58×10^{-3} mol) were dissolved in a 1-pentanol solution (10 mL) containing lithium, and the solution was refluxed for 1 h under nitrogen. After evaporation of the solvent, the residue was subjected to chromatography on silica gel with toluene as eluent and separated into two components: metal-free adjacently dibenzo-substituted TAP and a mixture of metal-free monobenzo-substituted and oppositely dibenzo-substituted TAPs. These metal-free compounds and an excess of zinc acetate were refluxed in DMF for 1 h, and the resultant Zn complexes purified on silica gel and Bio-beads gel (S-x1) columns with $CHCl_3$ as eluent. Recrystallization from $CHCl_3$/methanol produced **1Zn**, **2AdZn**, and **2OpZn** as green powders in 0.8% (15 mg), 3.3% (34 mg), and 0.7% (7 mg) yield, respectively. **1Zn**: FAB MS: *m*/*z*: 1140 $[M+1]^+$; elemental analysis (%) calcd for $C_{72}H_{66}N_8O_2Zn$: C 75.81, H 5.83, N 9.82; found: C 75.08, H 5.76, N 9.58; ^{1}H NMR (400 MHz, $CDCl_3$ + 1% C_5D_5N): $\delta = 8.69$ (s, 2H; ArH), 8.44 (d, 4H; *o*-Ph), 8.36 (m, 8H; *o*-Ph), 7.69 (t, 4H; *m*-Ph), 7.60–7.47 (m, 14H; *m*-Ph, *p*-Ph), 4.48 (t, 4H; OCH_2), 2.09 (quin, 4H; OCH_2CH_2), 1.68 (quin, 4H; $OCH_2CH_2CH_2$), 1.52–1.35 (m, 16H; $OCH_2CH_2CH_2CH_2CH_2CH_2CH_2$), 0.92 ppm (t, 6H; CH_3); **2AdZn**: FAB MS: *m*/*z*: 1294 $[M+1]^+$; elemental analysis (%) calcd for $C_{80}H_{92}N_8O_4Zn$: C 74.20, H 7.16, N 8.65; found: C 73.65, H 7.12, N 8.54; ^{1}H NMR (400 MHz, $CDCl_3$ + 1% C_5D_5N): $\delta = 8.86$ (s, 2H; ArH), 8.65 (s, 2H; ArH), 8.40 (d, 4H; *o*-Ph), 8.31 (d, 4H; *o*-Ph), 7.68–7.64 (m, 4H; *m*-Ph), 7.56–7.44 (m, 8H; *m*-Ph, *p*-Ph), 4.56 (t, 4H; OCH_2), 4.47 (t, 4H; OCH_2), 2.12–2.04 (m, 8H; OCH_2CH_2), 1.73–1.63 (m, 8H; $OCH_2CH_2CH_2$), 1.52–1.33 (m, 32H; $OCH_2CH_2CH_2CH_2CH_2CH_2CH_2$), 0.93–0.89 ppm (m, 12H; CH_3). **2OpZn**: FAB MS: *m*/*z*: 1294 $[M+1]^+$; elemental analysis (%) calcd for $C_{80}H_{92}N_8O_4Zn$: C 74.20, H 7.16, N 8.65; found: C 73.62, H 6.97, N 8.46; ^{1}H NMR (400 MHz, $CDCl_3$ + 1% C_5D_5N): $\delta = 8.70$ (s, 4H; ArH), 8.45 (d, 8H; *o*-Ph), 7.68 (t, 8H; *m*-Ph), 7.56 (t, 4H; *p*-Ph), 4.47 (t, 8H; OCH_2), 2.08 (quin, 8H; OCH_2CH_2), 1.67 (quin, 8H; $OCH_2CH_2CH_2$), 1.52–1.34 (m, 32H; $OCH_2CH_2CH_2CH_2CH_2CH_2CH_2$), 0.91 ppm (t, 12H; CH_3).

[2^2,2^3,7^2,7^3,12^2,12^3-Hexaoctyloxytribenzo[*b*,*g*,*l*]-17,18-diphenyl-5,10,15,20-tetraazaporphinato(2−)]zinc(II) (3Zn): Diphenylmaleonitrile[40] (80 mg, 3.5×10^{-4} mol) and 4,5-dioctyloxyphthalonitrile[42] (385 mg, 1.00×10^{-3} mol) were dissolved in a 1-pentanol solution (5 mL) containing lithium, and the solution refluxed for 1 h under nitrogen. After evaporation of the solvent, the residue was purified on silica gel (toluene as eluent) and Bio-beads gel (S-x1, $CHCl_3$ as eluent) columns to give metal-free tribenzo-substituted TAP. This metal-free compound and an excess of zinc acetate were refluxed in DMF for 1 h. The reaction mixture was purified on silica gel, Bio-beads gel (S-x1), and alumina columns with $CHCl_3$ as eluent. Recrystallization from $CHCl_3$/methanol afforded **3Zn** as a green powder in 5.3% yield (27 mg). FAB MS: *m*/*z*: 1449 $[M+1]^+$; elemental analysis (%) calcd for $C_{88}H_{118}N_8O_6Zn$: C 72.93, H 8.21, N 7.73; found: C 72.89, H 8.35, N 7.59; ^{1}H NMR (400 MHz, $CDCl_3$ + 1% C_5D_5N): $\delta = 8.91$ (s, 2H; ArH), 8.87 (s, 2H; ArH), 8.68 (s, 2H; ArH), 8.43 (d, 4H; *o*-Ph), 7.69–7.65 (t, 4H; *m*-Ph), 7.55 (t, 2H; *p*-Ph), 4.59 (m, 8H; OCH_2), 4.49 (t, 4H; OCH_2), 2.12 (quin, 12H; OCH_2CH_2), 1.71 (quin, 12H; $OCH_2CH_2CH_2$), 1.53–1.35 (m, 48H; $OCH_2CH_2CH_2CH_2CH_2CH_2CH_2$), 0.95–0.91 ppm (m, 18H; CH_3).

Octa-2,3,9,10,16,17,23,24-octyloxyphthalocyaninato(2−)zinc(II) (4Zn): A 1-pentanol solution containing lithium and 4,5-dioctyloxyphthalonitrile[42] (609 mg, 1.58×10^{-3} mol) was refluxed for 1 h under nitrogen. After addition of an excess of zinc acetate, the mixture was refluxed for 30 min. After evaporation of the solvent, the residue was subjected to chromatography over silica gel with $CHCl_3$ as eluent to give 35 mg (5.5% yield) of **4Zn** as a green powder. Elemental analysis (%) calcd for $C_{96}H_{144}N_8O_8Zn$: C 71.90, H 9.05, N 6.99; found: C 71.50, H 9.00, N 6.89; ^{1}H NMR (400 MHz, $CDCl_3$ + 1% C_5D_5N): $\delta =$ 8.95 (s, 8H; ArH), 4.62 (t, 16H; OCH_2), 2.15 (quin, 16H; OCH_2CH_2), 1.74 (quin, 16H; $OCH_2CH_2CH_2$), 1.57–1.34 (m, 64H; $OCH_2CH_2CH_2CH_2CH_2CH_2CH_2$), 0.93 ppm (t, 24H; CH_3).

[2^2,2^3-Dioctyloxybenzo[*b*]-7,8,12,13,17,18-hexa(*p*-*tert*-butylphenyl)-5,10,15,20-tetraazaporphinato(2−)]palladium(II) (1Pd): Bis(*p*-*tert*-butylphenyl)fumaronitrile[43] (110 mg, 3.21×10^{-4} mol) and 4,5-dioctyloxyphthalonitrile[42] (44 mg, 1.1×10^{-4} mol) were dissolved in a 1-pentanol solution (4 mL) containing lithium, and the solution refluxed for 1 h under nitrogen. After evaporation of the solvent, the residue was subjected to chromatography over silica gel with toluene and hexane/$CHCl_3$ (1/1) as eluents to give metal-free monobenzo-substituted TAP (24 mg). This metal-free compound and $PdCl_2$ (135 mg, 7.61×10^{-4} mol) were refluxed in chlorobenzene/DMF (1/1, 3 mL) for 2 h. After removal of the solvent by evaporation, the residue was purified on silica gel and Bio-beads gel (S-x1) columns with $CHCl_3$ as eluent. Recrystallization from $CHCl_3$/hexane yielded **1Pd** as a dark green powder in 9% yield (15 mg). ESI-TOF MS: *m*/*z*: 1518 $[M+1]^+$. Elemental analysis (%) calcd for $C_{96}H_{114}N_8O_2Pd$: C 75.94, H 7.57, N 7.38; found: C 75.69, H 7.62, N 7.24; ^{1}H NMR (400 MHz, $CDCl_3$): $\delta = 8.49$ (s, 2H; ArH), 8.26 (m, 12H; *o*-Ph), 7.70 (d, 4H; *m*-Ph), 7.58 (m, 8H; *m*-Ph), 4.40 (t, 4H; OCH_2), 2.08 (quin, 4H; OCH_2CH_2), 1.67 (quin, 4H; $OCH_2CH_2CH_2$), 1.55–1.37 (m, 70H; $OCH_2CH_2CH_2CH_2CH_2CH_2CH_2$, *t*Bu), 0.94 ppm (t, 6H; CH_3).

[2^2,2^3,7^2,7^3-Tetraoctyloxydibenzo[*b*,*g*]-12,13,17,18-tetra(*p*-*tert*-butylphenyl)-5,10,15,20-tetraazaporphinato(2−)]palladium(II) (2AdPd),

[2²,2³,12²,12³-tetraoctyloxydibenzo[*b*,*l*]-7,8,17,18-tetra(*p*-*tert*-butylphenyl)-5,10,15,20-tetraazaporphinato(2−)]palladium(II) (2OpPd), and [2²,2³,7²,7³,12²,12³-tetraoctyloxytribenzo[*b*,*g*,*l*]-17,18-bis(*p*-*tert*-butylphenyl)-5,10,15,20-tetraazaporphinato(2−)]palladium(II) (3Pd): Bis(*p*-*tert*-butylphenyl)fumaronitrile[43] (409 mg, 1.19×10^{-3} mol) and 4,5-dioctyloxyphthalonitrile[42] (249 mg, 6.47×10^{-4} mol) were dissolved in a 1-pentanol solution (12 mL) containing lithium, and the solution refluxed for 1 h under nitrogen. After removing the solvent, the residue was purified by silica gel (toluene, $CHCl_3$, and hexane/$CHCl_3$ as eluents) and Bio-beads gel (S-x1 or S-x2, $CHCl_3$ as eluent) columns, and separated into three fractions: metal-free oppositely dibenzo-, adjacently dibenzo-, and tribenzo-substituted TAPs. These metal-free compounds and $PdCl_2$ were refluxed in a mixed solution of chlorobenzene and DMF for 2 h. After evaporation of the solvent, the residue was purified on silica gel and Bio-beads gel (S-x1 or S-x2, $CHCl_3$ as eluent) columns, and by preparative TLC (silica, hexane/$CHCl_3$ as eluent). Recrystallization from $CHCl_3$/methanol gave **2OpPd**, **2AdPd**, and **3Pd** as dark blue powders in 2.7% (14 mg), 7.5% (38 mg), and 5.5% (19 mg) yield, respectively. **2AdPd**: ESI-TOF MS: $m/z=1560$ $[M+1]^+$; elemental analysis (%) calcd for $C_{96}H_{124}N_8O_4Pd$: C 73.89, H 8.01, N 7.18; found: C 73.69, H 8.18, N 7.22; ^{1}H NMR (400 MHz, $CDCl_3$): $\delta=8.51$ (br, 2H; ArH), 8.26–8.14 (br m, 10H; *o*-Ph, ArH), 7.69 (d, 4H; *m*-Ph), 7.51 (d, 4H; *m*-Ph), 4.45–4.30 (br m, 8H; OCH_2), 2.10 (br m, 8H; OCH_2CH_2), 1.73 (br m, 8H; $OCH_2CH_2CH_2$), 1.59–1.37 (br m, 68H; $OCH_2CH_2CH_2CH_2CH_2CH_2CH_2$, *t*Bu), 0.96 ppm (m, 12H; CH_3). **2OpPd**: ESI-TOF MS: m/z: 1560 $[M+1]^+$; elemental analysis (%) calcd for $C_{96}H_{124}N_8O_4Pd$: C 73.89, H 8.01, N 7.18; found: C 73.97, H 8.25, N 7.23; ^{1}H NMR (400 MHz, $CDCl_3$): $\delta=8.39$ (s, 4H; ArH), 8.30 (d, 8H; *o*-Ph), 7.68 (d, 8H; *m*-Ph), 4.45 (t, 8H; OCH_2), 2.13 (quin, 8H; OCH_2CH_2), 1.72 (quin, 8H; $OCH_2CH_2CH_2$), 1.59–1.39 (m, 68H; $OCH_2CH_2CH_2CH_2CH_2CH_2CH_2$, *t*Bu), 0.95 ppm (t, 12H; CH_3). **3Pd**; ESI-TOF MS: m/z: 1602 $[M+1]^+$; elemental analysis (%) calcd for $C_{96}H_{134}N_8O_6Pd$: C 71.95, H 8.43, N 6.99; found: C 71.63, H 8.25, N 7.09; ^{1}H NMR (400 MHz, $CDCl_3$): $\delta=8.40$ (br, 6H; ArH), 8.30 (d, 4H; *o*-Ph), 7.71 (d, 4H; *m*-Ph), 4.47 (br m, 12H; OCH_2), 2.15 (br m, 12H; OCH_2CH_2), 1.77 (br m, 12H; $OCH_2CH_2CH_2$), 1.60–1.40 (m, 66H; $OCH_2CH_2CH_2CH_2CH_2CH_2CH_2$, *t*Bu), 0.97 ppm (m, 18H; CH_3).

Acknowledgment

This work was partially carried out in the Advanced Instrumental Laboratory for Graduate Research of the Department of Chemistry, Graduate School of Science, Tohoku University, and was supported by a Grant-in-Aid for Young Scientists (Category A No. 14703007), Scientific Research in Priority Areas "Diagnosis and Treatment of Cancer" (No. 15025212 and 16023213), and the COE project, Giant Molecules and Complex Systems, 2004 from the Ministry of Education, Culture, Sports, Science and Technology, Japan.

[1] *Phthalocyanines—Properties and Applications*, *Vols. I–IV* (Eds.: C. C. Leznoff, A. B. P. Lever), VCH, New York, **1989**, **1992**, **1993**, **1996**.

[2] *Phthalocyanines—Chemistry and Functions* (Eds. H. Shirai, N. Kobayashi), IPC, Tokyo, **1997** (in Japanese).

[3] N. B. McKeown, *Phthalocyanine Materials Synthesis, Structure and Function*, Cambridge University Press, Cambridge, **1998**.

[4] *The Porphyrins*, *Vols. I–VII* (Ed. D. Dolphin), Academic Press, New York, **1978**, **1979**.

[5] *The Porphyrin Handbook*, *Vols. 1–10* (Eds.: K. M. Kadish, R. M. Smith, R. Guilard), Academic Press, New York, **2000**.

[6] *The Porphyrin Handbook*, *Vols. 11–20* (Eds. K. M. Kadish, R. M. Smith, R. Guilard), Academic Press, New York, **2003**.

[7] a) N. Kobayashi in *Phthalocyanines—Properties and Applications*, *Vol. 2* (Eds.: C. C. Leznoff, A. B. P. Lever), VCH, New York, **1992**, Chap. 3; b) N. Kobayashi, H. Konami in *Phthalocyanines—Properties and Applications Vol. 4* (Eds.: C. C. Leznoff, A. B. P. Lever), VCH, New York, **1996**, Chap. 9; c) N. Kobayashi in *The Porphyrin Handbook*, *Vol. 2* (Eds.: K. M. Kadish, R. M. Smith, R. Guilard), Academic Press, New York, **2000**, Chap. 13; d) N. Kobayashi in *The Porphyrin Handbook*, *Vol. 15* (Eds.: K. M. Kadish, R. M. Smith, R. Guilard), Academic Press, New York, **2003**, Chap 100.

[8] K. Ishii, N. Kobayashi in *The Porphyrin Handbook Vol. 16* (Eds.: K. M. Kadish, R. M. Smith, R. Guilard), Academic Press, New York, **2003**, Chap. 102.

[9] a) M. Zhao, C. Stern, A. G. M. Barrett, B. M. Hoffman, *Angew. Chem.* **2003**, *115*, 478; *Angew. Chem. Int. Ed.* **2003**, *42*, 462; b) S. I. Vagin, M. Hanack, *Eur. J. Org. Chem.* **2002**, 2859; c) S. L. J. Michel, D. P. Goldberg, C. Stern, A. G. M. Barrett, B. M. Hoffman, *J. Am. Chem. Soc.* **2001**, *123*, 4741; d) S. Lee, A. J. P. White, D. J. Williams, A. G. M. Barrett, B. M. Hoffman, *J. Org. Chem.* **2001**, *66*, 461; e) L. A. Ehrlich, P. J. Skrdra, W. K. Jarrel, J. W. Sibelt, N. R. Armstrong, S. S. Saavedra, A. G. M. Barrett, B. M. Hoffman, *Inorg. Chem.* **2000**, *39*, 3963; f) T. P. Forsyth, D. G. P. Williams, A. G. Montalban, C. L. Stern, A. G. M. Barrett, B. M. Hoffman, *J. Org. Chem.* **1998**, *63*, 331; g) T. F. Baumann, M. S. Nasier, J. W. Sibert, A. J. P. White, M. M. Olmstead, D. J. Williams, A. G. M. Barrett, B. M. Hoffman, *J. Am. Chem. Soc.* **1996**, *118*, 10479; h) M. Aoudia, G. Cheng, V. O. Kennedy, M. E. Kenney, M. A. J. Rodgers, *J. Am. Chem. Soc.* **1997**, *119*, 6029; i) B. L. Wheeler, G. Nagasubramanian, A. J. Bard, L. A. Schechtman, D. R. Dininny, M. E. Kenney, *J. Am. Chem. Soc.* **1984**, *106*, 7404.

[10] a) N. Kobayashi, R. Kondo, S. Nakajima, T. Osa, *J. Am. Chem. Soc.* **1990**, *112*, 9640; b) N. Kobayashi, T. Ishizaki, K. Ishii, H. Konami, *J. Am. Chem. Soc.* **1999**, *121*, 9096.

[11] a) N. Kobayashi, T. Ashida, T. Osa, *Chem. Lett.* **1992**, 2031; b) N. Kobayashi, T. Ashida, T. Osa, H. Konami, *Inorg. Chem.* **1994**, *33*, 1735; c) N. Kobayashi, M. Togashi, T. Osa, K. Ishii, S. Yamauchi, H. Hino, *J. Am. Chem. Soc.* **1996**, *118*, 1073; d) N. Kobayashi, H. Miwa, H. Isago, T. Tomura, *Inorg. Chem.* **1999**, *38*, 479; e) H. Miwa, E. A. Makarova, K. Ishii, E. A. Luk′yanets, N. Kobayashi, *Chem. Eur. J.* **2002**, *8*, 1082; f) N. Kobayashi, J. Mack, K. Ishii, M. J. Stillman, *Inorg. Chem.* **2002**, *41*, 5350.

[12] a) N. Kobayashi, T. Fukuda, *J. Am. Chem. Soc.* **2002**, *124*, 8007; b) N. Kobayashi, H. Miwa, V. N. Nemykin, *J. Am. Chem. Soc.* **2002**, *124*, 8021.

[13] a) M. S. Rodriguez-Morgade, G. de la Torre, T. Torres in *The Porphyrin Handbook*, *Vol. 15*, (Eds.: K. M. Kadish, R. M. Smith, R. Guilard), Academic Press, New York, **2003**, Chap. 99; b) C. G. Claessens, D. Gonzalez-Rodriguez, T. Torres, *Chem. Rev.* **2002**, *102*, 835; c) R. S. Iglesias, M. Segala, M. Nicolau, B. Cabezon, V. Stefani, T. Torres, P. R. Livotto, *J. Mater. Chem.* **2002**, *12*, 1256; d) M. K. Islyakin, M. S. Rodriguez-Morgade, T. Torres, *Eur. J. Org. Chem.* **2002**, 2460; e) M. Nicolau, B. Cabezon, T. Torres, *Coord. Chem. Rev.* **1999**, *190–192*, 231; f) F. Fernandez-Lazaro, T. Torres, B. Hauschel, M. Hanack, *Chem. Rev.* **1998**, *98*, 563.

[14] M. Gouterman in *The Porphyrins Vol. 3*, (Ed.: D. Dolphin), Academic Press, New York, **1978**, Chap. 1.

[15] A. B. P. Lever, E. R. Milaeva, G. Speier in *Phthalocyanines-Properties and Applications*, *Vol. 3* (Eds.: C. C. Leznoff, A. B. P. Lever), VCH, Weinheim, **1993**, Chap. 1.

[16] In the case of **2AdZn**, **2OpZn**, and **3Zn**, the first oxidation couple is reversible, but the first oxidation couple of **4Zn** seems to consist of two overlapping waves. Overlapping waves are often observed for aggregated Pcs. This was supported by CV measurements at various scan rates; the re-reduction wave at more anodic potential became more prominent at faster scan rates, while the less anodic counterpart diminished. Therefore, the more anodic wave is assigned to the monomer. The reduction couples are reversible except in the case of **2AdZn**. H. Isago, C. C. Leznoff, M. F. Ryan, R. A. Metcalfe, R. Davids, A. B. P. Lever, *Bull. Chem. Soc. Jpn.* **1998**, *71*, 1039.

[17] For all the zinc complexes, very weak absorption bands are observed between the Soret and Q bands. For Pcs with alkoxyl groups, these absorption bands are assigned to n–π* transitions. This broad band is also seen for **0Zn**, but not observed for tetra-*tert*-butylated ZnTAP. Therefore, the broad band of **0Zn** originates from transitions related to phenyl groups. This is supported by the CI calculations, which show that transitions at around 400 nm become more intense with increasing number of phenyl groups (Figure 12). a) N. Kobayashi, A. B. P. Lever, *J. Am. Chem. Soc.* **1987**, *109*, 7433; b) L. Guo, D. E. Ellis, B. M. Hoffman, Y. Ishikawa, *Inorg. Chem.* **1996**, *35*, 5304.

[18] a) J. Michl, *J. Am. Chem. Soc.* **1978**, *100*, 6801; b) J. Michl, *J. Am. Chem. Soc.* **1978**, *100*, 6812.
[19] a) W. R. Browett, M. J. Stillman, *J. Comput. Chem.* **1987**, *8*, 241; b) J. Mack, M. J. Stillman in *The Porphyrin Handbook*, *Vol. 16* (Eds.: K. M. Kadish, R. M. Smith, R. Guilard), Academic Press, New York, **2003**, Chap. 103; c) M. J. Stillman, T. Nyokong in *Phthalocyanines--Properties and Applications*, *Vol. 1* (Eds.: C. C. Leznoff, A. B. P. Lever), VCH, New York, **1989**, Chap. 3; d) M. J. Stillman in *Phthalocyanines-Properties and Applications*, *Vol. 3* (Eds.: C. C. Leznoff, A. B. P. Lever), VCH, New York, **1993**, Chap. 5; e) J. Mack, M. J. Stillman, *Coord. Chem. Rev.* **2001**, *219–221*, 993.
[20] Fitting parameters are summarized in the Supporting Information. Two closely lying Faraday *B* terms can be regarded as a pseudo-*A* term, and therefore the MCD bands of **2AdZn** were fitted by using either a Faraday *A* term or two *B* terms of opposite sign. Since a weak shoulder is seen at around 640–650 nm, the ΔE_{SS} value was evaluated as 280 cm^{-1} for **2AdZn**. a) A. Tajiri, Z. Winkler, *Z. Naturforsch. A* **1983**, *38*, 1263; b) A. Kaito, T. Nozawa, T. Yamamoto, M. Hatano, *Chem. Phys. Lett.* **1977**, *52*, 154.
[21] M. J. Stillman, A. J. Thompson, *J. Chem. Soc. Faraday Trans. 2* **1974**, *70*, 790.
[22] a) P. S. Vincett, E. M. Voigt, K. E. Rieckhoff, *J. Chem. Phys.* **1971**, *55*, 4131; b) S. S. Dvornikov, V. N. Knyukshto, V. A. Kuzmitsky, A. M. Shulga, K. N. Solovyov, *J. Lumin.* **1981**, *12*, 373.
[23] a) J. H. van der Waals, W. G. van Dorp, T. J. Schaafsma in *The Porphyrins*, *Vol. 4* (Ed.: D. Dolphin), Academic Press, New York, **1978**, Chap. 3; b) W. G. van Dorp, W. H. Schoemaker, M. Soma, J. H. van der Waals, *Mol. Phys.* **1975**, *30*, 1701; c) K. Ishii, T. Ishizaki, N. Kobayashi, *J. Phys. Chem. A* **1999**, *103*, 6060; d) K. Ishii, S. Abiko, N. Kobayashi, *Inorg. Chem.* **2000**, *39*, 468.
[24] For the PPP calculations, structures of pyrrole-deprotonated dianionic species were constructed by using X-ray structural data of Pc and by making the ring perfectly planar and adopting C_{2v}, D_{2h}, or D_{4h} symmetry.[7b] a) J. M. Robertson, I. Woodward, *J. Chem. Soc.* **1937**, 217; b) P. A. Barrett, C. E. Dent, R. P. Linstead, *J. Chem. Soc.* **1936**, 1719; c) C. J. Brown, *J. Chem. Soc. A* **1968**, *2488*, 2494; d) J. E. Kirner, W. Dow, J. R. Scheidt, *Inorg. Chem.* **1976**, *15*, 1685.
[25] MO and CI calculations were performed with the PM3 or ZINDO Hamiltonian by means of the program HyperChem. R.5.1. The π-conjugated systems of **0Zn** and **4Zn**, which were planar and of D_{4h} symmetry, were first optimized under the ZINDO/1 method. For **1Zn**, **2AdZn**, **2OpZn**, and **3Zn**, structures with elimination of the fused benzo rings from the optimized Pc were employed. Methoxyl groups optimized by the MM+ method were used instead of long alkoxyl chains, and the dihedral angle between the TAP plane and phenyl groups was assumed to be 35° by reference to the X-ray structural data. While the electronic structures are influenced by the distortion of a porphyrin plane, it was confirmed by the PM3 calculations that the TAP skelton was optimized to be planar even with the substitutions. a) N. Kobayashi, T. Fukuda, K. Ueno, H. Ogino, *J. Am. Chem. Soc.* **2001**, *123*, 10740; b) J. L. Retsek, S. Gentemann, C. J. Medforth, K. M. Smith, V. S. Chirvony, J. Fajer, D. Holten, *J. Phys. Chem. B* **2000**, *104*, 6690.
[26] Th zfs in the T_1 state was calculated under a half-point charge approximation employing the HOMO and LUMO coefficients obtained by the PPP calculations.[24] J. Higuchi, *J. Chem. Phys.* **1963**, *38*, 1237.
[27] S. R. Langhoff, E. R. Davidson, M. Gouterman, W. R. Leenstra, A. L. Kwiram, *J. Chem. Phys.* **1975**, *62*, 169.
[28] For various porphyrinic complexes, notable temperature dependence of the *E* value has been observed, since the signs of the *E* value are different for the T_{1x} and T_{1y} states.[23a] On the other hand, for **2AdZn**, a small temperature dependence of the *E* value are reasonably explained by the half-point charge calculations, in which the signs of the *E* value the same for the T_{1x} and T_{1y} states.
[29] K. Ishii, Y. Ohba, M. Iwaizumi, S. Yamauchi, *J. Phys. Chem.* **1996**, *100*, 3839.
[30] TREPR spectra of **3Pd** exhibited a concentration dependence due to aggregation, and therefore the TREPR measurement was carried out at low concentration (3×10^{-5} M).
[31] J. A. Kooter, G. W. Canters, J. H. van der Waals, *Mol. Phys.* **1977**, *33*, 1545.
[32] a) W. H. Chen, K. E. Rieckhoff, E. M. Voigt, *Chem. Phys.* **1985**, *95*, 123; b) W. H. Chen, K. E. Rieckhoff, E. M. Voigt, *Chem. Phys.* **1986**, *102*, 193.
[33] a) W. H. Chen, K. E. Rieckhoff, E. M. Voigt, *Mol. Phys.* **1986**, *59*, 355; b) W. A. J. A. van der Poel, A. M. Nuijs, J. H. van der Waals, *J. Phys. Chem.* **1986**, *90*, 1537.
[34] For **2AdZn**, nodes of the calculated b_1 and a_2 orbitals (LUMO and LUMO+1, respectively) lie along the *meso–meso* direction, in contrast to the other compounds (Figure 9). Since the LUMOs of **2AdZn** are degenerate, the LUMOs of **2AdZn** in Figure 10 are calculated as a linear combination of the b_1 and a_2 orbitals.
[35] T. M. Dunn, *Trans. Faraday Soc.* **1961**, *57*, 1441.
[36] Within the framework of the extended Hückel MO calculations, the *Z* values of the Pd complexes without substituents were calculated to be 44, 49, 43, 47, 42, and 42 cm^{-1} for **0Pd**, **1Pd**, **2AdPd**, **2OpPd**, **3Pd**, and **4Pd**, respectively.[35] These *Z* values are slightly larger than those obtained experimentally,[31,32] but the structural dependence is low (within 10%).
[37] K. Ishii, S. Takeuchi, S. Shimizu, N. Kobayashi, *J. Am. Chem. Soc.* **2004**, *126*, 2082.
[38] K. Ishii, J. Fujisawa, A. Adachi, S. Yamauchi, N. Kobayashi, *J. Am. Chem. Soc.* **1998**, *120*, 3152.
[39] K. Tominaga, S. Yamauchi, N. Hirota, *J. Phys. Chem.* **1990**, *94*, 4425.
[40] A. H. Cook, R. P. Linstead, *J. Chem. Soc.* **1937**, 929.
[41] N. Kobayashi, T. Ashida, K. Hiroya, T. Osa, *Chem. Lett.* **1992**, 1567.
[42] M. Hanack, P. Haish, H. Lehmann, L. R. Subramanian, *Synthesis* **1993**, 387.
[43] a) L. E. Marinina, S. A. Mikhalenko, E. A. Luk′yanets, *Zh. Obshch. Khim.* **1973**, *43*, 2025; b) T. F. Baumann, A. G. M. Barrett, B. M. Hoffman, *Inorg. Chem.* **1997**, *36*, 5661.

Received: April 4, 2004
Published online: July 27, 2004

